PML mutants resistant to arsenic induced degradation fail to generate the appropriate SUMO and ubiquitin signals required for RNF4 and p97 recruitment.

Ellis G. Jaffray, Michael H. Tatham, Alejandro Rojas-Fernandez, Adel Ibrahim, Graeme Ball and Ronald T. Hay*

Centre for Gene Regulation and Expression, School of Life Sciences, University of Dundee, Dundee, UK

***Corresponding author**

Email: r.t.hay@dundee.ac.uk

ORCID: 0000-0001-7113-9024

ABSTRACT

Arsenic is an effective treatment for Acute Promyelocytic Leukaemia as it induces degradation of the Promyelocytic Leukaemia (PML) – retinoic acid receptor alpha (RARA) oncogenic fusion protein. Some patients relapse with arsenic resistant disease because of missense mutations in PML. To determine the mechanistic basis for this arsenic resistance we reconstituted PML-/- cells with wild type (WT) and two mutant forms of YFP-PMLV found in patients refractory to arsenic, A216T and L217F. Both mutants formed PML bodies that were larger, but less numerous than WT and neither responded to arsenic by degradation. Analysis of immunoprecipitated PML bodies indicated that while WT PML experiences increased SUMO1, SUMO2/3 and ubiquitin conjugation, A216T PML is almost completely unresponsive and does not recruit the SUMO targeted ubiquitin E3 ligase RNF4. L217F PML was modified by SUMO and recruited RNF4, but failed to develop the the type of ubiquitin conjugate required to recruit the segregase p97, which is essential for PML degradation. Thus, the two PML mutants fail to be degraded as they do not acquire the necessary SUMO and ubiquitin signals required to progress through the degradation pathway.

INTRODUCTION

Acute Promyelocytic Leukaemia (APL) is caused by a reciprocal chromosomal translocation t(15;17) that fuses the genes encoding the Promyelocytic Leukaemia (PML) protein and the retinoic acid receptor alpha (RARA) (de The, Lavau et al. 1991, Kakizuka, Miller et al. 1991). This generates the PML-RARA oncoprotein that deregulates transcriptional programmes required for the differentiation of haematopoetic progenitor cells. As a consequence, differentiation is blocked and

promyelocytes accumulate causing leukaemia (Grignani, Ferrucci et al. 1993, Kwok, Zeisig et al. 2006, Martens, Brinkman et al. 2010, Mikesch, Gronemeyer et al. 2010, Tan, Wang et al. 2021). In healthy cells the PML gene is alternatively spliced to generate multiple mRNAs that encode seven protein isoforms (I-VII) that differ in their C-terminal regions.

PML is a member of the Tripartite Motif (TRIM) family of proteins and is also known as TRIM19. Located in the N-terminal region of PML and present in all PML isoforms and PML-RARA fusions, the highly conserved TRIM is composed of a RING domain, two zinc co-ordinating B-boxes and a coiled-coil that mediates dimerization (Bernardi and Pandolfi 2007). In cells with wild type (WT) PML genes, the protein is associated with non-membranous nuclear structures known as PML nuclear bodies, that also accumulate a variety of other proteins including Small Ubiquitin-like Modifiers (SUMOs), p53, Daxx and SP100. In cells containing a PML-RARA fusion protein, PML and PML-RARA are co-associated in a large number of tiny nuclear speckles (Dyck, Maul et al. 1994, Weis, Rambaud et al. 1994). In the past, treatment options were limited and APL was a disease with a very poor prognosis. However, the majority of patients are now cured by a combination therapy consisting of arsenic trioxide (referred to herein as As) and *all trans* retinoic acid (ATRA) (Wang and Chen 2008, Lo-Coco, Avvisati et al. 2013, Mi, Chen et al. 2015). These induce degradation of the PML-RARA oncogene and allows the WT version of RARA to initiate a transcriptional programme that drives the accumulated promyelocytes down a pathway of terminal differentiation that ultimately cures the disease. Arsenic alone induces degradation of both the unfused PML and PML-RARA, identifying PML as the target of As. Treatment with As leads to rapid multisite modification of PML and

PML-RARA with SUMO (Muller, Matunis et al. 1998). SUMO modified PML and PML-RARA then serves to recruit the SUMO Targeted Ubiquitin E3 ligase (STUbL) RING Finger Protein 4 (RNF4) (Perry, Tainer et al. 2008, Geoffroy and Hay 2009). Recruitment of RNF4 to SUMO modified PML and PML-RARA present in PML nuclear bodies is mediated by multiple SUMO Interaction Motifs (SIMs) present in the N-terminal region of the protein. The high local concentration of RNF4 leads to dimerization of the C-terminal RING domains and activation of the ubiquitin E3 ligase activity of the protein (Rojas-Fernandez, Plechanovova et al. 2014). RNF4 mediated ubiquitination of SUMO modified PML and PML-RARA ultimately leads to their proteolytic degradation by the proteasome (Lallemand-Breitenbach, Jeanne et al. 2008, Tatham, Geoffroy et al. 2008). Recently, an additional step required for arsenic induced degradation of PML and PML-RARA has been uncovered that involves the p97/VCP segregase (Jaffray, Tatham et al. 2023). RNF4 mediated ubiquitination of PML leads to recruitment of UFD1-NPLOC4-p97 which extracts ubiquitinated PML and presumably feeds the modified protein to the proteasome where it is proteolytically degraded.

While the majority of APL patients treated with As are cured, a small proportion of these patients relapse and present with arsenic resistant disease. In some cases resistance may be a consequence of metabolic reprogramming linked to expression of additional known oncogenes (Madan, Shyamsunder et al. 2016, Iaccarino, Ottone et al. 2019), but in many patients, arsenic resistance is a result of missense mutations in PML clustered between residues L211 and S220 in B-box 2. These mutations are not only found in the PML-RARA oncogene (Goto, Tomita et al. 2011, Chendamarai, Ganesan et al. 2015, Lou, Ma et al. 2015, Iaccarino, Ottone et al.

2016, Liu, Zhu et al. 2016) but also in the unfused version of PML (Lehmann-Che, Bally et al. 2014, Zhu, Qin et al. 2014, Iaccarino, Ottone et al. 2016). These mutations are undetectable at initial diagnosis, suggesting that cells expressing these mutations are selected for by arsenic treatment (Alfonso, Iaccarino et al. 2019, Balasundaram, Ganesan et al. 2022).

To establish the mechanistic basis for the arsenic resistance we investigated the properties of two mutations in PML that responded differently to As. While both mutations were resistant to As-induced degradation, the A216T mutant was severely compromised for SUMO modification, failed to recruit RNF4 and as a result was not ubiquitinated. In contrast the L217F mutant was SUMO modified in response to ATO, recruited RNF4 and was efficiently ubiquitinated. However, the ubiquitin signal was not sufficient to recruit the p97 segregase that is required to extract PML from nuclear bodies. Thus, two mutations that are adjacent in the PML B-box have very different responses to ATO: A216T fails to accrue the appropriate SUMO signal required to recruit RNF4, whereas L217F is SUMO modified and ubiquitinated, but the signal is not recognised by the p97 segregase.

RESULTS

PML mutants A216T and L217F form atypical PML bodies in U2OS cells.

Mutations in PML and PML-RARA that arise in APL patients with arsenic resistant disease are a unique resource as these mutations are selected in vivo to be resistant to arsenic while still retaining the biological functions of PML that contribute to the disease phenotype. The majority of these mutations are located to a 10 amino acid region (L211-S220) of the B-box 2 of PML that encompasses, but never includes, the

zinc co-ordinating residues C212 and C215 (Fig. 1A). As PML is the direct target of arsenic and mutations from patients with arsenic resistant disease can also be detected in the non-rearranged allele of PML (Lehmann-Che, Bally et al. 2014, Iaccarino, Ottone et al. 2016), we chose to reconstitute U2OS PML-/- cells with wild-type (WT) or mutant versions of PMLV N-terminally fused to YFP (Jaffray, Tatham et al. 2023). In testing a number of PML variants, we found that they fell into two main groups exemplified by the most frequently identified mutation in patients A216T and L217F. U2OS cells expressing YFP fused forms of WT, A216T and L217F PMLV were isolated by FACS and the derived cell lines analysed by high content microscopy. Images of these cells show that while the total YFP fluorescence signal was similar for WT, A216T and L217F, the size and number of PML bodies per cell varied among WT, A216T and L217F (Fig. 1B). Quantitative analysis of thousands of cells showed that the average expression levels, measured by YFP-PML intensity per cell, were similar for all three PML forms (Fig. 1C). However, cells expressing A216T and L217F PMLV had on average approximately half the number of PML bodies per cell (median = 4) compared to WT (median = 8) (Fig. 1C). This was contrasted by both mutants showing larger than WT PML bodies according to their measured area (Fig. 1C). This ~20-25% larger cross-sectional area equates to almost twice the volume when considering a spherical PML body. These results show that A216T and L217F mutations to PML reduce PML body number and increase PML body size in untreated cells.

PML mutants A216T and L217F are not degraded in response to arsenic in U2OS cells

Arsenic exposure is responsible for dramatic changes to the number, morphology and content of PML bodies (Geoffroy et al., 2010; Jeanne et al., 2010). To determine how these parameters were influenced by mutations in PML, the cells expressing WT, A216T or L217F YFP-PMLV were either untreated or treated with 1μM arsenic and monitored by time-lapse fluorescence microscopy over a 15 hr period. At least 9 movies were collected for each condition and an automated, quantitative pipeline (Jaffray et al., 2023) was used to follow PML body size, number and total YFP-PMLV fluorescence intensity over time (see Supplementary movies 1-6 for representative time-course data). Images from the same cells at 0 and 15 hr (Fig. 2A) showed the expected reduction in the number and total intensity of nuclear bodies in WT PMLV expressing cells, but not in cells expressing A216T or L217F PMLV (Fig. 2A). Averaged vales of these metrics across all time courses indicated that PML body size did not significantly change over time after arsenic treatment for any of the PML forms studied (Fig. 2B). Furthermore, the number of bodies per cell and normalized YFP-PML intensity was reduced during arsenic exposure for WT PML but not for either mutant (Fig. 2B). More specifically, after 15 hr As there was a >4 fold reduction in the number of PML bodies per cell and >3 fold reduction in YFP-PMLV intensity for the WT PMLV, while little or no change was observed for A216T and L217F mutants (Fig. 2C). Western-blot analysis of extracts gathered from cells exposed to arsenic over a 24 hr time-course showed that as expected, WT PML rapidly shifts to a higher molecular weight species and is completely degraded by 24 hr (Fig. 2D). In contrast, A216T PML does not appear to shift to a higher molecular weight form and its levels do not change over the 24 hr period. Unlike A216T, L217F PML does shift to higher molecular weight species, but it is not degraded in response to arsenic after 24 hr (Fig. 2D).

In response to arsenic WT and L217F PML recruit RNF4 but the A216T mutant does not

Although A216T does not appear to respond to arsenic by altered post-translational modification, both the WT and L217F forms display reduced electrophoretic mobility upon exposure of cells to arsenic (Fig. 2D). To better understand the nature of the modification status of all PML variants, nuclear bodies were purified from WT, A216T and L217F YFP-PMLV expressing cells (Jaffray, Tatham et al. 2023) both before and after treatment with 1μM As for 2h and analysed by Western blot for PML, SUMO1 or SUMO2/3. Consistent with the analysis of PML from whole cell extracts (Fig. 2D), purified YFP-PMLV WT and L217F shifted to higher molecular weight species in response to arsenic treatment for 2 hrs, whereas this response was almost completely absent for A216T (Fig. 3A). SUMO1 modification of all three PML forms in untreated cells appears to be similar, but in response to arsenic, WT YFP-PMLV undergoes a much greater increase in SUMO1 modification than either A216T or L217F mutants. As with SUMO1, in untreated cells conjugation of all three PML forms to SUMO2/3 is broadly comparable (Fig. 3A), however the relative increase upon arsenic exposure in SUMO2/3 conjugation for WT PML appears to be smaller than for SUMO1. The increase in SUMO2/3 conjugation for the mutants was more comparable with WT PML than for SUMO1, although the A216T mutant is the most defective, showing only a modest increase in SUMO2/3 conjugation (Fig. 3A). Enhanced SUMO modification of PML is responsible for the recruitment of the STUbL RNF4 that mediates PML ubiquitination prior to degradation by the proteasome. To study RNF4 recruitment in response to arsenic, nuclear bodies from WT, A216T and L217F YFP-PMLV expressing cells were again purified and the

associated RNF4 determined by Western blotting (Fig. 3B). RNF4 was not stably associated with nuclear bodies in the absence of arsenic, but was detected in purifications containing WT and L217F YFP-PMLV forms after arsenic treatment (Fig. 3B). By this analysis RNF4 was not detectable in A216T YFP-PMLV purifications in response to arsenic (Fig. 3B). The YFP-PMLV purifications were then analysed for ubiquitin modification by Western blotting with an antibody that detects ubiquitin chains. This revealed that WT YFP-PMLV was extensively ubiquitinated in response to arsenic and, consistent with the failure to recruit RNF4, increase in the ubiquitination of A216T YFP-PMLV was not detected (Fig. 3B). Interestingly, although L217F YFP-PMLV recruited RNF4, the increase in ubiquitin chains was not a large as for the WT protein, and the modified species had a lower molecular weight (Fig. 3B).

The arsenic-induced recruitment of SUMO1, SUMO2/3 and RNF4 to PML bodies was also analysed by fluorescence microscopy for the three different cell lines. This confirmed that colocalization of SUMO1, SUMO2/3 and RNF4 with PML was increased for the WT protein in response to arsenic (Supplementary Figs. 1-3). Consistent with the Western blot data (Fig. 3A+B), the A216T PML mutant showed little response to arsenic in terms of recruitment of SUMO1, SUMO2/3 or RNF4. The L217F PML variant showed lower than WT recruitment of SUMO1 and SUMO2/3 in response to arsenic (Supplementary Fig. 1&2), although RNF4 levels appeared similar (Supplementary Fig. 3). In this experiment, RNF4 appears to colocalise with PML nuclear bodies prior to arsenic treatment, but this increases in response to arsenic for both WT and L217F and less so for A216T (Supplementary Fig. 3). Thus, both Western blotting and fluorescence microscopy indicate that the inability of

A216T PML to be degraded is the consequence of the failure in SUMO modification to recruit RNF4, and therefore is not ubiquitinated. This was not the case for L217F which could recruit RNF4 and induce ubiquitination, but was still resistant to degradation.

In response to arsenic L217F PML fails to recruit the p97 segregase

Recently we determined that the p97 segregase was required to extract ubiquitinated PML from nuclear bodies prior to degradation by the proteasome (Jaffray, Tatham et al. 2023). To determine if the mutants were compromised for p97 extraction we analysed WT, A216T and L217F YFP-PMLV expressing cells by fluorescence microscopy 0, 2, 4 and 6 hr after arsenic treatment. p97 recruitment was determined by evaluating the extent of co-localisation between antibody stained p97 and PML marked by YFP fluorescence. As p97 is a highly abundant protein we employed a pre-extraction procedure to release the bulk of the soluble p97 from the cells before fixation. In WT YFP-PMLV untreated cells p97 was associated with only a small proportion of PML bodies, whereas after 6 hr arsenic treatment a larger fraction of PML bodies had associated p97 (Supplementary Fig. 4). In cells expressing A216T and L217F YFP-PMLV, arsenic treatment did not appear to increase the association of p97 with PML bodies (Fig. 4A, Supplementary Fig. 4). To quantify this the percentage of PML bodies co-localised with p97 in WT, A216T and L217F YFP-PMLV expressing cells was determined at 0, 2, 4 and 6 hr after arsenic treatment (Fig. 4B). In untreated WT YFP-PMLV expressing cells about 20% of PML bodies were associated with p97, which increased to over 60% at 2, 4 and 6 hr after arsenic treatment. In untreated cells expressing A216T and L217F YFP-PMLV, p97 association was less than 10% and this did not increase in response to arsenic (Fig.

4B). Statistical analysis of the 0 hr and 6 hr time-points data revealed that there was a substantial and statistically significant recruitment of p97 to PML bodies in cells expressing WT YFP-PMLV, but not in cells expressing A216T or L217F YFP-PMLV (Fig. 4C). Changes in the expression levels of p97 in the different cell lines, or upon arsenic treatment could not explain these differences (Supplementary Fig. 5). Thus, although L217F YFP-PMLV recruits SUMO and RNF4 to generate ubiquitin conjugates, this signal is not sufficient to engage p97, and therefore proteasomal degradation fails.

A216T and L217F mutants of PML differ from WT in their post-translational modification with SUMO and ubiquitin

To provide more detail on the post-translational modifications that accumulate on PML, we repeated the purification of YFP-PML nuclear bodies with a view to release SUMO or ubiquitin from resin-bound material by treatment with proteases specific for each (Supplementary Fig. 6A). The material released by protease treatment, and that remaining on the beads can be analysed by Western blotting, which should provide information not only on the covalent modification status of PML, but also that of the SUMO1, SUMO2/3 and ubiquitin species attached to PML (Supplementary Fig. 6B). Prior to purification, nuclear extracts for WT, A216T and L217F YFP-PMLV displayed the expected changes in electrophoretic mobility (Supplementary Fig. 6C), and were almost completely depleted from nuclear extracts after YFP-PML purification. Importantly, the modifications to PML were preserved during purification (Fig. 5A “No protease”). For all PML variants treatment of the beads with SENP1 returned most of the heavier PML forms back to more rapidly migrating species consistent with unmodified YFP-PMLV (Fig. 5 “SENP1” lanes). Treatment with USP2 had little impact

on the distribution of PML species, indicating only a relatively small proportion of the modified PML is ubiquitin conjugated (Fig. 5A “USP2”). SUMO1 blots show that in untreated cells there are relatively low levels of SUMO1 associated with PML, while after arsenic treatment this increases dramatically for WT YFP-PMLV, modestly for L217F YFP-PMLV, and not at all for A216T YFP-PMLV (Fig. 5B). As expected, these species disappear upon SENP1 treatment, but are largely unaltered by treatment with USP2 (Fig. 5B). The arsenic-induced change to SUMO2/3 modification is not as extreme as for SUMO1, but WT and L217F YFP-PMLV both display increased SUMO2/3 modification (Fig. 5C). Unlike with SUMO-1, there is a small but detectable increase in the SUMO2/3 modification of A216T (Fig. 5C). SUMO2/3 is also completely removed by SENP1, but USP2 treatment does not result in significant changes to SUMO2/3 antibody reactive species (Fig. 5C). Blotting with an antibody to ubiquitin reveals that it is present at low levels on WT, A216T and L217F YFP-PMLV in untreated cells but is dramatically increased on in WT, modestly increased on L217F but any increase on A216T is imperceptible in this assay (Fig. 5D). For both WT PML and the L217F mutant, SENP1 treatment not only reduces the amount of ubiquitin remaining on the beads, it causes the ubiquitin-reactive species to run at a reduced molecular weight (Fig. 5D). This ubiquitin released by SENP1 is probably that conjugated directly to SUMO, while the material remaining is directly conjugated to PML. As expected, ubiquitin is removed from purifications by treatment with USP2 (Fig. 5D). Although ubiquitination of L217F in response to arsenic is less than that of WT YFP-PMLV, it is still far more substantial than the A216T mutant (Fig. 5D).

The material released from the bead-associated YFP-PMLV by treatment with the proteases was also analysed by Western blotting. As expected, none of the treatments released YFP-PMLV (Supplementary Fig. 7A). SENP1 treatment released low levels

of monomeric SUMO1 from untreated WT and L217F YFP-PMLV samples, with none detected from A216T purifications. After arsenic treatment the amount of SUMO1 released by SENP1 from WT samples increased for both WT and L217F PML forms, albeit less extensively for the mutant. Compared to these two, the amount of SUMO1 conjugated to A216T after arsenic exposure was negligible although it was at least detectable compared to the sample derived from untreated cells (Supp. Fig. 7B). SENP1 of WT-PML purifications also released forms of SUMO1 shifted up around 10kDa from the unmodified SUMO1 species, which are presumed to be SUMO1 conjugated by ubiquitin, as they are sensitive to USP2 (Supplementary Fig. 7B). However, these species were not apparent in SENP1 elutions from L217F-PML purifications according to this assay, implying ubiquitination of SUMO1 is most common in WT-PML. SENP1 digestion released substantial amounts of monomeric SUMO2/3 from preparations derived from untreated cells for all PML variants including A216T (Supp. Fig. 7C). Arsenic treatment induced a modest increase in SUMO2/3 conjugates on all three PML forms, although a SUMOylated form of SUMO2/3 was only apparent for WT and L217F variants (Supp. Fig. 7C). These SUMO-ubiquitin hybrid species released by SENP1 were also detected using a ubiquitin antibody (Supplementary Fig. 7D). Although data shown in Fig. 5C suggest SUMO2/3 modification of PML low prior to arsenic and increases after arsenic treatment, this is not consistent with analysis of the material released by SENP1 treatment (Supplementary Fig. 6C) which shows similar SUMO2/3 amounts both before and after arsenic. A possible explanation for this apparent discrepancy is that in untreated cells the SUMO2/3 modified PML are dispersed throughout the gel, whereas after SENP1 treatment all of the SUMO2/3 is collapsed into a single species. Which of these two is the more reliable is not clear, therefore a more quantitative approach will help

resolve this anomaly.

In summary, A216T YFP-PMLV is defective for arsenic induced SUMO1, SUMO2/3 and ubiquitin modification. L217F YFP-PMLV appears to be partially compromised for SUMO2/3 conjugation but more compromised for SUMO1 conjugation. Furthermore, WT PML shows higher levels of direct ubiquitination than L217F, whereas L217F ubiquitination appears to mostly take place on SUMO2/3 linked to PML. Finally, a significant proportion of SUMO1 conjugated to WT-PML is covalently conjugated by ubiquitin, while this was not detected for L217F PML.

Quantitative proteomic analysis of PML post-translational modifications in response to arsenic

Early descriptions of PML modification by SUMO identified three major acceptors at lysines 65, 160 and 490 (Kamitani, Kito et al. 1998). More recently, the single largest SUMO site proteomic analysis to date (Hendriks, Lyon et al. 2017) described a total of 15 acceptor lysines in PML (Supplementary figure 8A). To provide quantitative data at the amino-acid site level for the post-translational modifications present in PML and SUMO, a peptide-level quantitative proteomics analysis was undertaken. Trypsin digestion leaves long SUMO adducts attached to modified lysines (Supplementary Fig 8B), that are challenging to identify by mass-spectrometry. Thus, a strategy combining GluC digestion and trypsin digestion was employed to give shorter peptide fragments. As GluC is less specific and less stable than trypsin, multiple GluC adducts from SUMOs remain on lysines after digestion (Supplementary Fig. 8B), which has the advantage of providing multiple peptide evidences for a single modification.

Cultures of U2OS PML-/- +YFP-PML cells were grown for the WT, A216T and L217F PML variants, and were either treated or not with 1μM arsenic for 2 hr (Supplementary Fig. 9A). Four experimental replicates for each condition were prepared and YFP-PML purified by the same method as described above. Purifications were analysed by SDS-PAGE (Supplementary Fig. 9B) and the uppermost section of the gel containing proteins larger than 100kDa, including YFP-PML, was processed for mass-spectrometry analysis. Anti-PML Western blot of a fraction of the inputs revealed the YFP-PML proteins responded as expected to arsenic treatment (Supplementary Fig. 9C). 21 phosphorylation, 14 SUMOylation and 11 ubiquitination sites were identified in PML (Supplementary datafile 1 and Supplementary Fig. 10A). Principal component analysis using intensity data for all modified and unmodified peptides from YFP-PML, SUMO1, SUMO2, SUMO3 and ubiquitin shows replicates cluster by experimental condition and are clearly separated from one-another (Supplementary Fig. 10B), indicating clear differences among the conditions. Intensity data for all peptides were normalized by total YFP peptide intensity (Supplementary Fig. 10C), nomalize away any systematic errors relating to PML expression or loading (Supplementary Fig. 10D). Using the total intensity of the unmodified peptides from SUMO1, SUMO2/3 and ubiquitin as a proxy for their overall protein abundance (Supplementary Fig. 10E-G), a remarkably similar picture to that revealed in the Western blot experiments above (Fig. 3) was found: Prior to exposure to arsenic all three PML forms are associated with broadly similar amounts of SUMO1, SUMO2/3 and ubiquitin. Arsenic treatment has little effect on the modification of the A216T mutant, but triggers increased conjugation by SUMO1, SUMO2/3 and ubiquitin for WT and L217F PML, with the mutant showing a slightly weaker response. Also consistent with the Western blot data is the finding that

SUMO1 has a larger relative increase (5 fold) than SUMO2/3 (1.8 fold) in conjugation to WT PML after arsenic treatment. To allow the data from different peptides to be presented in a single plot, raw peptide intensities were normalized to relative intensity values (Supplementary Fig. 10H), which can be plotted in a single compact radial chart to summarise large amounts of quantitative data in a single plot (Fig. 6A).

WT PML becomes modified by SUMO1 and polymers containing SUMO1 after arsenic treatment

10 SUMO1 modifications to PML had relaible enough data for comparisons among conditions (Fig. 6B). After arsenic treatment WT PML was much more extensively modified with SUMO1 than either mutant at all PML sites except K160 in B-Box1, which appeared to be more occupied by SUMO1 in the L217F mutant (Fig. 6B). A216T PML was relativly unresponsive in SUMO1 conjugation. The results for SUMO2/3 were less clear-cut (Fig. 6C). Firstly, the scale of the difference among the three PML forms in the SUMO2 conjugation is much smaller than for SUMO1. Surprisingly, two of the 12 sites with good enough data for quantitative comparisons were most highly modified in the otherwise inert A216T mutant (Fig. 6C). These were K226 close to the mutation hotspot and K487 in the NLS (Fig. 6C). Several other sites in or around the NLS, K400, K476, and K497, showed greater modification for L217F than WT PML (Fig. 6C). The WT protein only clearly showed the most extensive SUMO2/3 modification at K380 (between the coiled-coil and NLS) and marginally higher conjugation at three sites; K65 (RING domain), K426 and K460 (both between the coiled-coil and the NLS). Site-level analysis of SUMO-SUMO branched peptides showed again that A216T PML was almost completely

unresponsive (Fig. 6D). SUMO polymers did accumulate on L217F PML, but not to the same extent as for WT PML (Fig. 6D). Notably all bar one of the identified SUMO-SUMO linages contained SUMO1 as conjugate donor, acceptor or both, so considering SUMO1 was recruited to WT PML more than L217F, this result is perhaps not very surprising. Together these results show arsenic induces high levels of SUMO1 conjugation to WT PML which is either abrogated or blunted in the two mutants of PML. SUMO2/3 conjugation is less severely impeded.

Neither A216T nor L217F PML is conjugated to polyubiquitin chains in response to arsenic

Of the 11 ubiquitination sites identified in PML, the majority were sites also identified as SUMO acceptors, except K183 between B-Boxes 1 and 2 and K337 in the coiled-coil domain. 9 sites had high quality quantitative data which showed that A216T essentially did not respond to arsenic with increased ubiquitination (Fig. 6E). In general WT and L217F PML showed similar overall increases in ubiquitination on PML although there were differences at the site level. Notably both A216T and L217F PML were much more highly modified at lysines 160 and 490 than WT (Fig. 6E). These are two of the three sites originally identified as major SUMO acceptors, and likely to already have relatively high occupancy. K183 and K337 were more occupied by ubiquitin in WT PML than either mutant (Fig. 6E). Ubiquitination of SUMO shows a striking difference between WT PML and the L217F mutant (Fig. 6F). This shows that the SUMO associated with L217F PML is much more extensively ubiquitinated than that conjugated to WT PML (Fig. 6F). in contrast to this, four of the five ubiquitin-ubiquitin branch specific peptides with good enough data to make quantitative comparisons were most abundant in WT PML preps (Fig.

6G). These results show that compared with WT PML, arsenic-induced ubiquitination of L217F PML is skewed towards SUMO ubiquitination, and away from ubiquitin-ubiquitin polymer formation.

DISCUSSION

The overarching cellular mechanisms governing arsenic-induced degradation of PML and the oncogenic fusion PML-RARA were broadly characterised more than ten years ago (Lallemand-Breitenbach, Jeanne et al. 2008, Tatham, Geoffroy et al. 2008). Arsenic triggers the SUMOylation of PML, followed by its ubiquitination, then degradation by the proteasome. However, the precise molecular signals required at each step are only partially understood, and new cellular players are still being discovered (Jaffray, Tatham et al. 2023). The functional characterisation of mutant forms of PML and PML-RAR found in APL patients refractory to arsenic treatment, provides an opportunity to better understand the biochemical details of arsenic-induced PML degradation. We have used a combination of high content, time-lapse microscopy and detailed peptide-level proteomic analysis to study two common patient-derived PML mutants A216T and L217F. We generated three model U2OS cell lines lacking endogenous PML but expressing YFP fusions of WT PML, A216T PML or L217F PML and found the two mutants were stable when cells were exposed to 1μM arsenic for 24 hours, while the WT protein was completely degraded. In untreated cells, there are few differences among them with WT PML and both mutants carrying relatively comparable amounts of SUMO1, SMO2/3 and ubiquitin. Although the mutations are in adjacent amino-acids and neither protein was degraded, arsenic triggered quite different post-translational modification responses on each. After 2 hours exposure of 1μM arsenic compared to WT PML, A216T PML

showed no great increase in either SUMOylation or ubiquitination. However, arsenic did trigger large increases in SUMO and ubiquitin modification in L217F PML, albeit to a lesser degree than for WT PML. The simplest explanation for these results is that each step of the PML degradation pathway has a threshold requirement of SUMO and ubiquitin accumulation which must be met to progress towards degradation, and A216T does not accumulate enough SUMO, while L217F does not accumulate enough ubiquitin. Indeed, we found YFP-PML A216T did not colocalise with the SUMO specific Ubiquitin ligase RNF4 required for arsenic induced degradation of PML, and while the L217F mutant did recruit RNF4, it did not colocalise with the p97 segregase required to extract ubiquitinated PML from PML bodies prior to degradation. WT PML colocalised with both under the same conditions.

However, analysis of PML modifications at the site levels using proteomics showed that it may not simply be the quantity of SUMO or ubiquitin that is important, but the nature of these signals. The most revealing comparisons in this regard were between WT PML and the partially responsive L217F mutant. Total amounts of SUMO2/3 associated with WT and L217F PML were similar, but more than twice as much SUMO1 was recruited to WT PML bodies than the mutant equivalents. After arsenic treatment, SUMO1 modification on WT PML was more extensive than the mutant at all PML sites detected except K160, which was modestly more conjugated in L217F PML. In contrast, overall SUMO2/3 modification of PML was of a similar scale for both L217F and WT proteins, with most lysines showing similar responses for both PML forms and only a small number differing significantly between the PML types. While it cannot be excluded that defective or excessive SUMO2/3 modification at specific sites in L217F PML explains its resistance to degradation, it seems more

likely that it is sub-optimal SUMO1 conjugation that negatively affects L217F during the later stages of arsenic induced degradation. This seems counter-intuitive as RNF4 is poly-SUMO specific (Tatham, Geoffroy et al. 2008), and unlike SUMO2/3, SUMO1 lacks the SUMOylation conjugation consensus motif that readily facilitates SUMO polymerisation in SUMO2/3 (Tatham, Jaffray et al. 2001). However, SUMO1 has been shown to be SUMOylated in vivo on non-consensus lysines (Tammsalu, Matic et al. 2014, Hendriks, Lyon et al. 2017), and even in absence of this conjugate 'acceptor' function, SUMO1 can still contribute to SUMO polymers as a conjugate 'donor' molecule. Evidence for this was found in our proteomic data which showed after arsenic treatment, much more SUMO1-SUMO-2 and SUMO1-SUMO3 conjugates accumulated on WT PML than either mutant. It is also possible that extensive monomeric SUMOylation conjugation could engage and activate RNF4 if enough SUMOs are in close proximity (Aguilar-Martinez and Sharrocks 2016). This may be more possible for a protein like PML which forms multimeric complexes and contains numerous SUMOylation sites. We also cannot exclude the possibility that a novel effector protein with preference for SUMO1 over SUMO2/3 contributes to the creation of the appropriate polyubiquitin signal required to recruit p97.

Our data do suggest there are differences between WT PML and L217F in the nature of the ubiquitin conjugates triggered by arsenic. On PML itself K160 and K490 seem to be far stronger acceptors of ubiquitin for L217F PML, than WT. This may be a consequence of lower availability of K160 and K490 in WT PML, as the unmodified peptides containing both lysines are much less abundant for WT PML than for L217F (Supp. Fig. 11A). Conversely K183 in B-Box 2 and K337 at the end of the Coiled-coil show greater ubiquitin occupancy for WT PML. Notably neither K183 nor K387 were

detectably modified by SUMO according to our proteomic analysis, and to our knowledge neither has been identified as a SUMO acceptor in any large-scale proteomics analyses. Therefore it could be the case that ubiquitination at either of these sites is crucial for p97 recruitment.

Even though less SUMO is conjugated to L217F PML than the WT, ubiquitination of SUMOs is much more extensive for the mutant. This ‘over ubiquitination’ of SUMOs by L217F appears to come at the cost of the formation of ubiquitin polymers, which were only found to accrue on WT PML (Supplementary Fig. 11B). Even for WT-PML, the increases in abundance of the Ub-Ub branch-specific peptides during arsenic treatment is relatively modest, however two factors may have bearing upon this. Firstly, this experiment was conducted after only 2 hours of arsenic treatment, and it is possible longer exposures may increase the abundance of Ub-Ub polymers. Secondly, it is likely that once the correct polyubiquitin signal is developed on PML, p97 may rapidly process it for degradation, making the actual signal for degradation short lived and difficult to detect. It is noteworthy that of the five ubiquitin-ubiquitin linkage-specific peptides detected, K11, K33 and K48 met statistical cutoffs to be described as significantly increase after arsenic treatment. (Supplementary Fig. 11B). p97 recognises polyubiquitin chains containing 5 or more copies of ubiquitin (Twomey, Ji et al. 2019), and both K11 and K48 linkages are implicated in p97 function (Locke, Toth et al. 2014, Meyer and Rape 2014, Yau, Doerner et al. 2017), thus it seems most likely that defective ubiquitin polymerisation associated with L217F PML has the greatest potential to explain the lack of p97 recruitment and hence, degradation.

In summary, two patient-derived mutant forms of PML, A216T and L217F result in similar clinical aetiologies but have subtly different biochemical responses to arsenic resulting in blocked degradation (See Supplementary figure 12). A216T is almost completely unresponsive to arsenic experiencing only very modest changes in SUMOylation and ubiquitination, most likely because it does not engage the appropriate SUMO conjugation machinery. L217F PML becomes modified with both SUMO1 and SUMO2, but while ubiquitination is stimulated, it does not create the appropriate ubiquitin-containing signal required to recruit p97 needed to extract modified PML prior to degradation by the proteasome. These findings begin to question the simplicity of the current stochastic model for SUMO and ubiquitin-mediated degradation of PML and raise the prospect of the involvement of more as yet unidentified players in the PML degradation pathway.

MATERIALS AND METHODS

Preparation of anti-GFP nanobody magnetic beads. 300mg of Dynabeads M-270 Epoxy (ThermoFisher Scientific Catalogue No. 14302D) were resuspended in 10 ml of 0.1 M sodium phosphate buffer pH 7.5 and washed twice using a DynaMag-15 magnet (ThermoFisher Scientific Catalogue No. 12301D) with 10 ml of the same buffer. 4 mg of the LaG16 nanobody that recognises GFP (Fridy, Li et al. 2014) in 10 ml of 1 M $(NH_4)_2SO_4$, 0.1 M sodium phosphate buffer pH 8.0 was added to the beads which were incubated overnight at 27ºC with end over end rotation. After coupling was complete the beads were washed 6 times with phosphate buffered saline (PBS) and stored in PBS, 0.1% NaN_3 at 4^0C.

Purification of YFP-PML from U2OS PML-/- YFP-PML cells. For each 'replicate' of the proteomics experiment five 15 cm diameter plates of approximately 80% confluent cells were used. Prior to harvesting, growth medium was removed and cells washed in situ twice with 5mL PBS/100mM iodoacetamide. For each dish, cells were scraped into 5mL PBS+100mM iodoacetamide and transferred to a 50mL tube. A second 2mL volume of PBS+100mM iodoacetamide was used to clean the plate of all cells and pooled with the first 5mL. This was repeated for all dishes for each replicate and pooled in the same 50mL tube (~35mL total). Cells were pelleted by centrifugation at 400g for 5 minutes at 22ºC and resuspended in 10 mL 4ºC hypotonic buffer including iodoacetamide (10mM HEPES pH 7.9, 1.5mM MgCl2, 10mM KCl, 0.08% NP-40, 1x EDTA-free protease inhibitor cocktail (Roche), + 100mM Iodoacetamide). A sample of this may be retained as a "Whole cell extract". These were snap-frozen in liquid nitrogen and stored at -80ºC until required. Cells were thawed by tube rotation at 4ºC for 30 minutes. Tubes were then centrifuged at 2000g, 4ºC for 10 minutes to pellet nuclei. Supernatants were discarded but a sample of this can be taken as a "Cytosolic fraction". Each pellet of nuclei was resuspended in 5mL ice-cold hypotonic buffer containing 20mM DTT but without iodoacetamide, transferred to a 15mL tube and centrifuged at 2000g, 4ºC for 10 minutes. The nuclei were washed once more in 5mL ice-cold hypotonic buffer (without iodoacetamide or DTT) and the supernatant discarded. To digest DNA, nuclei were resuspended in 5mL "Buffer A" (50mM Tris pH 7.5, 150mM NaCl, 0.2mM DTT, 1µg/ml benzonase, 1x EDTA-free protease inhibitor cocktail (Roche)) and incubated on ice for 15 minutes. Samples were sonicated in 15mL tubes on ice (Branson Sonifier) using the small probe, 6 cycles of 30 seconds at approximately 50% amplitude with at least 2 minutes cooling on ice in between cycles. PML bodies should remain intact at this point. Insoluble debris was removed

by centrifugation at 1200g for 20 minutes at 4ºC, and the supernatant containing soluble PML bodies, transferred to a new 15ml centrifuge tube. A sample of this can be taken as a “Nuclear fraction”. To each 5mL supernatant 6mL “Buffer B” was added (50mM Tris pH 7.5, 1% Triton-X-100, 0.1% Deoxycholic acid, 1x EDTA-free protease inhibitor cocktail (Roche)). To each 11mL solution, 1mL volume of a 5% beads:buffer slurry (v:v) of magnetic anti-GFP nanobody beads, pre-equilibrated in 1:1.4 Buffer A:B mix (v:v), was added and mixed on a tube roller at 4ºC for 16h (50μL beads per sample). Using the DynaMag rack (Thermofisher scientific) the beads were extracted from suspension and the supernatant removed. A sample of this can be analysed to ensure YFP-PML depletion. Beads were then washed with 5mL “Buffer C” (50mM Tris pH 7.5, 500mM NaCl, 0.2mM DTT) and the beads extracted. These beads were then resuspended in 1mL “Buffer D” (50mM Tris pH 7.5, 150mM NaCl, 0.2mM DTT) and transferred to a new 1.5mL protein LoBind tube (Eppendorf) and after bead separation, washed once more with 1mL Buffer D. One half of this final sample of beads (25μL beads) was eluted for proteomic analysis by adding 35µl 1.2X NuPAGE LDS sample buffer (Thermofisher scientific), and incubated at 70ºC for 15 minutes with agitation, followed by fractionation by SDS-PAGE. If Western blot analysis was also required, the second half of the resin (25μL) would be resuspended in 250µl 1.2X NuPAGE LDS sample buffer (Thermo) and incubated at 70ºC for 15 minutes with agitation. Approximately 30µl would be used per gel lane. If treatment with proteases was required to monitor PML modification status, then the second half volume of beads (25μL) was divided into four and treated as follows: 1-Add 150 µl Buffer D. 2-Add 150 µl 250nM SENP1 in Buffer D. 3- Add 150 µl 500nM USP2 in Buffer D. 4- Add 150 µl 250nM SENP1/500nM USP2 in Buffer D. All tubes were agitated for 1-2 hrs at 22ºC,

supernatants removed (and can be kept for analysis) and beads washed twice with 1mL buffer D before elution with 250 µl 1.2X LDS, 70ºC, 15 minutes with agitation.

Proteomic analysis of YFP-PML purifications. Elutions from anti-GFP nanobody beads in 1.2x LDS/60mM DTT protein sample buffer were fractionated on 4-12% polyacrylamide Bis-Tris NuPAGE gels (Thermofisher Scientific) using MOPS running buffer. After Coomassie staining and destaining gels were excised into 4 slices per lane and tryptic peptides extracted from top slice (>100kDa) as previously described (Shevchenko, Tomas et al. 2006). Peptides were resuspended in 40µL 0.1% TFA 0.5% acetic acid and half STAGE tip purified prior to digestion with GluC. This gave two fractions per replicate: Trypsin digested, and Trypsin+GluC digested. 6µL of each was analysed by LC-MS/MS. This was performed using a Q Exactive mass spectrometer (Thermofisher Scientific) coupled to an EASY-nLC 1000 liquid chromatography system (Thermofisher Scientific), using an EASY-Spray ion source (Thermofisher Scientific) running a 75 µm x 500 mm EASY-Spray column at 45ºC. A 150 minute elution gradient with a top 8 data-dependent method was applied. Full scan spectra (m/z 300–1800) were acquired with resolution R = 70,000 at m/z 200 (after accumulation to a target value of 1,000,000 ions with maximum injection time of 20 ms). The 8 most intense ions were fragmented by HCD and measured with a resolution of R = 17,500 at m/z 200 (target value of 500,000 ions and maximum injection time of 120 ms) and intensity threshold of 2.1×10^4. Peptide match was set to 'preferred', a 40 second dynamic exclusion list was applied and ions were ignored if they had unassigned charge state 1, 8 or >8.

MS data were processed in MaxQuant version 1.6.1.0 (Cox and Mann 2008, Cox, Neuhauser et al. 2011). Multiple MaxQuant runs were performed considering multiple

SUMO1 and SUMO2/3 derived adducts as variable modifications (see Supplementary Datafile 1 for details), as well as those typical for ubiquitin and phosphorylation to Ser and Thr residues. A MaxQuant search for SUMO adducts was also conducted using a concatenated database approach using linear peptide fusions of SUMO C-termini to substrate peptides as search library (Matic, van Hagen et al. 2008). Oxidised methionine and acetylated protein N-termini were also selected as variable modifications and carbamidomethyl-C was the only fixed modification. Maximum number of variable modifications was set to 4. The match between runs option was enabled, which matches identified peaks among slices from the same position in the gel as well as one slice higher or lower. The uniport human proteome database (downloaded 19/4/2019 - 73920 entries) digested with Trypsin/P (maximum missed cleavages was 5) was used as search space. LFQ intensities were required for each slice. All FDR filtering was set to 1%. For peptides derived from GluC digestions 8 maximum missed cleavages were considered. Raw peptide intensities were manually normalized by the total YFP peptide intensity for each sample. Mass spectrometry data from samples derived from the same replicate were numerically summed to provide a final normalized peptide intensity for each identification in each sample. Downstream data processing used Perseus v1.6.1.1 (Tyanova, Temu et al. 2016). Zero intensity values were replaced from $\log_2$ transformed data (width 0.3 and downshift 1.8).

Pre-extraction of cells. Cells were grown on coverslips in 24 well plates. Coverslips were washed twice with PBS before being exposed to pre-extraction buffer (25 mM HEPES pH 7.4, 50 mM NaCl, 3 mM MgCl2, 0.5% Triton-X-100, 0.3M Sucrose) for 10 min. Cells were then processed through the procedure below for immunofluorescence.

Immunofluorescence analysis. Adherent cells were washed three times with PBS, fixed with 4% Formaldehyde in PBS for 15mins, then washed again three times with PBS before blocking for 30 min in 5% BSA, 0.1% TWEEN 20 in PBS. Fixed cells were washed once with 1% BSA, 0.1% TWEEN 20 in PBS before incubation for 1-2 hr with primary antibody in 1% BSA, 0.1% TWEEN 20 in PBS. These were chicken anti-PML (in house) and sheep anti-p97 (MRC Dundee). After 3 washes in 1% BSA, 0.1% TWEEN 20 in PBS cells were incubated with secondary antibody in 1% BSA, 0.1% TWEEN 20 in PBS for 60 min., washed three times in 1% BSA, 0.1% TWEEN 20 in PBS and stained with 0.1µg/ml DAPI for 2 min. These were Alexa Fluor (Invitrogen) Donkey anti-chicken 594, donkey anti-sheep 594 and donkey anti-chicken 488. Cover slips were rinsed twice with PBS, twice with water and dried before mounting in MOWIOL. Images were collected using a DeltaVision DV3 widefield microscope and processed using Softworx (both Applied Precision, Issaquah, WA). Images are presented as maximal intensity projections using Omero software. For quantitative p97-PML colocalization analysis the same image settings were applied across all fields and PML bodes per cell were counted for between 20 and 40 cells per condition. P97 colocalisation was defined as any p97 signal above background within the same region as a PML body. Percent colocalization was then calculated for each cell.

Live-Cell Imaging in Real Time and Measurement of Fluorescence Intensities. For all live-cell imaging experiments, cells were seeded onto µ-slide 8 well glass bottom (Ibidi 80827). Immediately prior to imaging cell medium was replaced with DMEM minus phenol red (gibco 31053-038) supplemented with 2mM glutamine and 10% fetal bovine serum. Cells were untreated or treated with 1µM arsenic. Time-laspe

microscopy was performed on a DeltaVision Elite restoration microscope (Cytiva) fitted with an incubation chamber (Solent Scientific) set to 37 ºC and 5% CO2 and a cooled charge-coupled device camera (CoolSnap HQ; Roper). SoftWorx software was used for image collection. Datasets were deconvolved using the constrained iterative algorithm (Swedlow, Sedat et al. 1996, Wallace, Schaefer et al. 2001) using SoftWorx software. Using a YFP specific filter set (Ex510/10nm, Em537/26nm), 5 z-planes spaced at 2 µm were taken every 15 min. A single brightfield reference image was taken at each time point to monitor cell health. Time courses were presented as maximum intensity projections of deconvolved 3D datasets. Movies were created in OMERO using the deconvolved images.

Quantitative analysis of PML body composition during Live-Cell imaging

Batch analysis of time-lapse movies was carried out using ImageJ (Schneider, Rasband et al. 2012) macros in Fiji (Schindelin, Arganda-Carreras et al. 2012) (Supplementary Materials). Briefly: 1) datasets (deconvolved with SoftWoRx) were cropped to remove border artefacts, 2) for each timepoint the maximum focus slice was selected according to intensity variance (radius 2 pixels), 3) auto-thresholding was performed using a threshold of mean intensity + 3 standard deviations, and 4) ImageJ's built-in "Analyze Particles" function was used to measure PML body count, size, total area, and intensity. Results were aggregated and summarized using R scripts as described previously (Jaffray, Tatham et al. 2023).

Preparation of cell extracts and Western blotting. Adherent cells were washed with PBS and lysed by the addition of 1.2X LDS buffer and heated to 70ºC for 10 min. Cell lysates were sonicated using a probe sonicator for two bursts of 30 sec. Samples were

run on NuPage 3-8% or 4-12% Bis-Tris precast gels (ThermoFisher Scientific) and transferred to nitrocellulose. Membranes were blocked in PBS with 5% non-fat milk and 0.1% Tween-20. Primary antibody incubations were performed in PBS with 3% BSA and 0.1% Tween-20. For the HRP-coupled secondary antibody incubations 5% milk was used instead of the BSA. The signal was detected by Pierce enhanced chemiluminescence (ThermoFisher scientific 32106) and X-ray films. Antibodies. Chicken anti-PML (homemade), sheep anti-SUMO-1 (homemade), rabbit anti-SUMO-2 (Cell signaling 4971S), rabbit FK2 ubiquitin (Enzo BML-PW8810-0500), rabbit anti-p97 (Abcam ab109240). HRP-coupled secondary anti-mouse, anti-rabbit anti-chicken and anti-sheep were purchased from Sigma.

FIGURE LEGENDS

Figure 1. Characterization of PML bodies in U2OS PML-/- cell lines expressing YFP-fusions of WT, A216T and L217F forms of PML-V. A. Schematic depiction of PML-V primary structure indicating the major domains, regions of common mutations associated with arsenic treatment resistance, and the common breakpoints leading to PML-RARA fusions. B. Representative images of the indicated PML-/- U2OS + YFP-PML-V cell lines C. High content imaging data summarizing the calculated values for total PML intensity per cell, PML body number per cell and area per PML body for each cell line. Scatter plots are shown with median (solid line) and quartiles (error bars). n=38411 (wt), 35210 (A216T) and 41288 (L217F).

Figure 2. A216T and L217F mutants of PML are not rapidly degraded in response to arsenic treatment in vitro. A. YFP fluorescence image stills from one live cell analysis of each YFP-PML cell type at both 0h and 15h treatment with 1μM

arsenic. B. Averaged data of 9 or 10 fields of view (median 12 cells per field) followed over a 15 hour time course of treatment or not with 1μM arsenic (15 minute intervals). Intensity measurements are normalized by the t=0hr values. C. Summary statistics (n=9 or 10) for 15hr data comparing 1μM arsenic treated cells with untreated cells. P-values are unpaired, two-tailed student's T-tests using Welch's correction for unequal variances where appropriate (§). See Supplementary movie files 1-6 for real-time data of a single representative field. D. Anti-PML Western-blots of fractionated whole cell extracts showing time-courses of the response of YFP-PML-V variants to 1μM arsenic exposure over 24 hours.

Figure 3. In response to arsenic A216T PML fails to recruit RNF4. Two separate purifications of YFP-PMLV WT, A216T and L217F (A+B): PML bodies were enriched from U2OS PML-/- + YFP-PMLV WT, A216T or L217F cells, either nontreated (NT) or treated with 1μM arsenic (1μM As 2h) for 2 hr. Bound material was eluted and analysed by Western blotting using antibodies to (A) PML, SUMO1, SUMO2/3 and (B) PML, RNF4 and ubiquitin.

Figure 4. A216T and L217F mutants of PML do not recruit p97 in response to arsenic treatment. A. Immunofluorescence images showing YFP-PMLV and p97 in the indicated cell lines after 6 hours arsenic treatment. Data showing merged images for these and the 0h time-point data can be seen in supplementary figure 4. B. Quantitative summary of p97 colocalization with PML bodies in the indicated cell lines during 0h, 2h, 4h and 6h arsenic exposure. Markers show average values and error bars are standard error of the mean. C. Statistical analysis of the comparison between 0h and 6h arsenic exposure for PML-p97 colocalization. Columns represent

average % colocalization, error bars are standard error of the mean, cell count is shown in brackets below each column and student's two-tailed t-test p-values are shown above.

Figure 5. Failure of arsenic resistant mutants to generate the SUMO and ubiquitin modified intermediates required for degradation. PML bodies were enriched from U2OS PML-/- + YFP-PMLV WT, A216T or L217F cells, either untreated (-) or treated with 1μM arsenic (+) for 2 hr. Purified PML bodies bound to anti-GFP nanobody magnetic beads were either untreated (No protease), treated with SUMO specific protease (SENP1), treated with ubiquitin specific protease (USP2) or a combination of both (USP2 + SENP1). Material remaining bound to the beads after treatment was eluted and analysed by Western blotting using antibodies to A. PML, B. SUMO1, C. SUMO2/3 and D. ubiquitin.

Figure 6. Differential site-specific modifications of WT, A216T and L217F PML forms before and after arsenic. PML bodies were enriched from U2OS PML-/- + YFP-PMLV WT, A216T or L217F cells and quantitatively analysed by mass spectrometry for protein content and site-specific modifications by SUMO1, SUMO2/3 and ubiquitin. A-G. Radial plots showing relative intensity for each of the indicated proteins or peptides. A. is derived from the total of the unmodified peptides for YFP, PML, SUMO1, SUMO2/3 and ubiquitin and is a proxy for of total protein abundance. Circles indicate the upper limit of the range, with the maximum relative intensity in brackets.

Supplementary Figure 1. Arsenic-induced colocalisation of SUMO1 with WT, A216T and L217F forms of YFP-PML. Colocalisation of SUMO1 with WT, A216T and L217F PML variants after 1μM arsenic treatment for 2h studied by fluorescence microscopy. Scale bar is 10μm.

Supplementary Figure 2. Arsenic-induced SUMO2/3 colocalisation with WT, A216T and L217F forms of YFP-PML. Colocalisation of SUMO2/3 with WT, A216T and L217F PML variants after 1μM arsenic treatment for 2h studied by fluorescence microscopy. Scale bar is 10μm.

Supplementary Figure 3. Arsenic-induced RNF4 colocalisation with WT, A216T and L217F forms of YFP-PML. Colocalisation of RNF4 with WT, A216T and L217F PML variants after 1μM arsenic treatment for 2h studied by fluorescence microscopy. Scale bar is 10μm.

Supplementary Figure 4. Arsenic-induced p97 colocalisation with WT, A216T and L217F forms of YFP-PML. Representative immunofluorescence images for 1μM arsenic treated YFP-PMLV cells at 0 hr and 6 hr. Monochrome images for YFP-PML and p97 channels are shown along with the merge of YFP-PMLV (green) and p97 (red) with DAPI (blue).

Supplementary Figure 5. p97 expression levels do not differ between cell types or upon arsenic treatment. Western blots for p97 and PML of whole cell extracts from the indicated cell lines either treated or not with arsenic.

Supplementary Figure 6. Treatment of purified PML bodies with recombinant SUMO and Ubiquitin proteases reveals the nature of PML post-translational modifications. A. Overview of the experimental design for detection of ubiquitin and SUMO conjugated to PML. B. Anti-PML Western blot for nuclear extracts from the indicated cell lines before and after purification of YFP-PML with GFP nanobody beads. C. Schematic depiction of the contents of YFP-PML bound to beads and resulting supernatants after treatment with specific proteases.

Supplementary Figure 7. Western blot analysis of the material eluted by SENP1 and USP2 from the purified YFP-PML forms indicated. Associated with Figure 5. Western blots using antibodies specific for PML (A), SUMO1 (B), SUMO2/3 (C) and ubiquitin (D). 2ng standards of recombinant proteins (Rec.) were included with the gels. The positions of recombinant PML (Rec.PML), unmodified forms of YFP-PML, SUMO1, SUMO2 and ubiquitin are indicated, along with ubiquitinated species (*).

Supplementary Figure 8. Known sites of PML SUMOylation and potential peptide adducts remaining on substrates after trypsin and GluC digestion. A. Positions of previously identified SUMO conjugation sites relative to the structural domains in PML. Isoform V is shown although identifications could be from other isoforms. Data taken from Hendriks et al 2017 (Hendriks, Lyon et al. 2017). Common breakpoints found in the PML-RARA and mutational hotspots found in arsenic insensitive forms are indicated. B. Overview of the potential remnants of SUMO C-termini attached to substrate lysine residues (K) when conjugates are cleaved by Trypsin, or GluC considering multiple missed cleavages.

Supplementary Figure 9. A proteomic study to quantitatively analyse arsenic-induced changes to PML post-translational modifications at the site level. A. Overview of the proteomic experimental design. B. Coomassie-stained gel showing the elutions from anti-GFP nanobody purifications for each replicate. Gel slices are numbered. C. Anti-PML western blot of a fraction of the anti-GFP nanobody purifications for each replicate.

Supplementary Figure 10. Overview of the proteomic data for the post-translational modification of PML WT, A216T and L217F

A. Summary of SUMO and ubiquitin conjugation sites identified in this study. Region of mutation hotspots is boxed. B. Principal component analysis of the quantitative proteomic data using only peptides from YFP-PML, SUMOs or ubiquitin. These included all unmodified peptides, phospho peptides, Ubiquitin branches and SUMO branches on YFP-PML, SUMO1, SUMO2/3 and Ubiquitin. Total is 343 peptides and uses $\log_2$ transformed and zero-replaced intensity values. C-G. Total unmodified peptide intensity data for the indicted proteins. Bars are average intensities with standard deviation error bars. p values are for two tailed student's t-test comparing untreated with arsenic treated samples. n=4. H. Summary of the data shown in C-G normalized by the average intensity for each protein.

Supplementary Figure 11. Column plots of relative peptide intensity data for selected peptide types. A. Unmodified counterpart peptides to the indicated sites of SUMOylation in PML. B. Ubiquitin-Ubiquitin linkage specific peptides. Columns are average values with SD error bars. Student's t-test p-values are indicated.

Supplementary Figure 12. Schematic summary of the arsenic-induced responses of WT, A216T and L217F forms of PML. WT, A216T and L217F forms of PML are modified by broadly similar amounts of SUMO1 and SUMO2/3 in untreated cells. Exposure of cells to arsenic triggers an increase in SUMO2/3 conjugation for WT PML and L217F PML, and a much smaller increase for A216T PML. A large increase in SUMO1 conjugation is triggered for WT PML, with a smaller increase for L217F PML, and no significant SUMO1 change for A216T. Arsenic does not induce increased ubiquitination of A216T, while L217F experiences increased ubiquitination to PML and SUMO proteins. WT PML also becomes ubiquitinated on PML and SUMOs, but a fraction also forms ubiquitin-ubiquitin polymers. Neither A216T PML nor L217F PML develop the requisite SUMO and/or ubiquitin signals required to bind p97 and target them for degradation.

REFERENCES

Aguilar-Martinez, E. and A. D. Sharrocks (2016). "The Use of Multimeric Protein Scaffolds for Identifying Multi-SUMO Binding Proteins." Methods Mol Biol **1475**: 195-204.

Alfonso, V., L. Iaccarino, T. Ottone, L. Cicconi, S. Lavorgna, M. Divona, R. Cairoli, A. Cristiano, C. Ciardi, S. Travaglini, G. Falconi, S. K. Hasan, A. Venditti, W. Arcese, M. T. Voso and F. Lo-Coco (2019). "Early and sensitive detection of PML-A216V mutation by droplet digital PCR in ATO-resistant acute promyelocytic leukemia." Leukemia **33**(6): 1527-1530.

Balasundaram, N., S. Ganesan, E. Chendamarai, H. K. Palani, A. Venkatraman, A. A. Alex, S. David, S. P. Kumar, N. R. Radhakrishnan, M. Yasar, S. Krishna, A. Korula, U. Kulkarni, N. B. Janet, P. Balasubramanian and V. Mathews (2022). "Metabolic adaptation drives arsenic trioxide resistance in acute promyelocytic leukemia." Blood Adv **6**(2): 652-663.

Bernardi, R. and P. P. Pandolfi (2007). "Structure, dynamics and functions of promyelocytic leukaemia nuclear bodies." Nat Rev Mol Cell Biol **8**(12): 1006-1016.

Chendamarai, E., S. Ganesan, A. A. Alex, V. Kamath, S. C. Nair, A. J. Nellickal, N. B. Janet, V. Srivastava, K. M. Lakshmi, A. Viswabandya, A. Abraham, M. Aiyaz, N. Mullapudi, R. Mugasimangalam, R. A. Padua, C. Chomienne, M. Chandy, A. Srivastava, B. George, P. Balasubramanian and V. Mathews (2015). "Comparison of newly diagnosed and relapsed patients with acute promyelocytic leukemia treated with arsenic trioxide: insight into mechanisms of resistance." PLoS One **10**(3): e0121912.

Cox, J. and M. Mann (2008). "MaxQuant enables high peptide identification rates, individualized p.p.b.-range mass accuracies and proteome-wide protein quantification." Nat Biotechnol **26**(12): 1367-1372.

Cox, J., N. Neuhauser, A. Michalski, R. A. Scheltema, J. V. Olsen and M. Mann (2011). "Andromeda: a peptide search engine integrated into the MaxQuant environment." J Proteome Res **10**(4): 1794-1805.
de The, H., C. Lavau, A. Marchio, C. Chomienne, L. Degos and A. Dejean (1991). "The PML-RAR alpha fusion mRNA generated by the t(15;17) translocation in acute promyelocytic leukemia encodes a functionally altered RAR." Cell **66**(4): 675-684.
Dyck, J. A., G. G. Maul, W. H. Miller, Jr., J. D. Chen, A. Kakizuka and R. M. Evans (1994). "A novel macromolecular structure is a target of the promyelocyte-retinoic acid receptor oncoprotein." Cell **76**(2): 333-343.
Fridy, P. C., Y. Li, S. Keegan, M. K. Thompson, I. Nudelman, J. F. Scheid, M. Oeffinger, M. C. Nussenzweig, D. Fenyo, B. T. Chait and M. P. Rout (2014). "A robust pipeline for rapid production of versatile nanobody repertoires." Nat Methods **11**(12): 1253-1260.
Geoffroy, M. C. and R. T. Hay (2009). "An additional role for SUMO in ubiquitin-mediated proteolysis." Nat Rev Mol Cell Biol **10**(8): 564-568.
Goto, E., A. Tomita, F. Hayakawa, A. Atsumi, H. Kiyoi and T. Naoe (2011). "Missense mutations in PML-RARA are critical for the lack of responsiveness to arsenic trioxide treatment." Blood **118**(6): 1600-1609.
Grignani, F., P. F. Ferrucci, U. Testa, G. Talamo, M. Fagioli, M. Alcalay, A. Mencarelli, F. Grignani, C. Peschle, I. Nicoletti and et al. (1993). "The acute promyelocytic leukemia-specific PML-RAR alpha fusion protein inhibits differentiation and promotes survival of myeloid precursor cells." Cell **74**(3): 423-431.
Hendriks, I. A., D. Lyon, C. Young, L. J. Jensen, A. C. Vertegaal and M. L. Nielsen (2017). "Site-specific mapping of the human SUMO proteome reveals co-modification with phosphorylation." Nat Struct Mol Biol **24**(3): 325-336.
Iaccarino, L., T. Ottone, V. Alfonso, L. Cicconi, M. Divona, S. Lavorgna, S. Travaglini, A. Ferrantini, G. Falconi, C. Baer, M. Usai, F. Forghieri, A. Venditti, M. I. Del Principe, W. Arcese, M. T. Voso, T. Haferlach and F. Lo-Coco (2019). "Mutational landscape of patients with acute promyelocytic leukemia at diagnosis and relapse." Am J Hematol **94**(10): 1091-1097.
Iaccarino, L., T. Ottone, M. Divona, L. Cicconi, R. Cairoli, M. T. Voso and F. Lo-Coco (2016). "Mutations affecting both the rearranged and the unrearranged PML alleles in refractory acute promyelocytic leukaemia." Br J Haematol **172**(6): 909-913.
Jaffray, E. G., M. H. Tatham, B. Mojsa, M. Liczmanska, A. Rojas-Fernandez, Y. Yin, G. Ball and R. T. Hay (2023). "The p97/VCP segregase is essential for arsenic induced degradation of PML and the PML-RARA oncoprotein." Journal of Cell Biology **In Press**.
Kakizuka, A., W. H. Miller, Jr., K. Umesono, R. P. Warrell, Jr., S. R. Frankel, V. V. Murty, E. Dmitrovsky and R. M. Evans (1991). "Chromosomal translocation t(15;17) in human acute promyelocytic leukemia fuses RAR alpha with a novel putative transcription factor, PML." Cell **66**(4): 663-674.
Kamitani, T., K. Kito, H. P. Nguyen, H. Wada, T. Fukuda-Kamitani and E. T. Yeh (1998). "Identification of three major sentrinization sites in PML." J Biol Chem **273**(41): 26675-26682.
Kwok, C., B. B. Zeisig, S. Dong and C. W. So (2006). "Forced homo-oligomerization of RARalpha leads to transformation of primary hematopoietic cells." Cancer Cell **9**(2): 95-108.
Lallemand-Breitenbach, V., M. Jeanne, S. Benhenda, R. Nasr, M. Lei, L. Peres, J. Zhou, J. Zhu, B. Raught and H. de The (2008). "Arsenic degrades PML or PML-RARalpha through a SUMO-triggered RNF4/ubiquitin-mediated pathway." Nat Cell Biol **10**(5): 547-555.

Lehmann-Che, J., C. Bally and H. de The (2014). "Resistance to therapy in acute promyelocytic leukemia." N Engl J Med **371**(12): 1170-1172.
Liu, J., H. H. Zhu, H. Jiang, Q. Jiang and X. J. Huang (2016). "Varying responses of PML-RARA with different genetic mutations to arsenic trioxide." Blood **127**(2): 243-250.
Lo-Coco, F., G. Avvisati, M. Vignetti, C. Thiede, S. M. Orlando, S. Iacobelli, F. Ferrara, P. Fazi, L. Cicconi, E. Di Bona, G. Specchia, S. Sica, M. Divona, A. Levis, W. Fiedler, E. Cerqui, M. Breccia, G. Fioritoni, H. R. Salih, M. Cazzola, L. Melillo, A. M. Carella, C. H. Brandts, E. Morra, M. von Lilienfeld-Toal, B. Hertenstein, M. Wattad, M. Lubbert, M. Hanel, N. Schmitz, H. Link, M. G. Kropp, A. Rambaldi, G. La Nasa, M. Luppi, F. Ciceri, O. Finizio, A. Venditti, F. Fabbiano, K. Dohner, M. Sauer, A. Ganser, S. Amadori, F. Mandelli, H. Dohner, G. Ehninger, R. F. Schlenk, U. Platzbecker, d. A. Gruppo Italiano Malattie Ematologiche, G. German-Austrian Acute Myeloid Leukemia Study and L. Study Alliance (2013). "Retinoic acid and arsenic trioxide for acute promyelocytic leukemia." N Engl J Med **369**(2): 111-121.
Locke, M., J. I. Toth and M. D. Petroski (2014). "Lys11- and Lys48-linked ubiquitin chains interact with p97 during endoplasmic-reticulum-associated degradation." Biochem J **459**(1): 205-216.
Lou, Y., Y. Ma, J. Sun, X. Ye, H. Pan, Y. Wang, W. Qian, H. Meng, W. Mai, J. He, H. Tong and J. Jin (2015). "Evaluating frequency of PML-RARA mutations and conferring resistance to arsenic trioxide-based therapy in relapsed acute promyelocytic leukemia patients." Ann Hematol **94**(11): 1829-1837.
Madan, V., P. Shyamsunder, L. Han, A. Mayakonda, Y. Nagata, J. Sundaresan, D. Kanojia, K. Yoshida, S. Ganesan, N. Hattori, N. Fulton, K. T. Tan, T. Alpermann, M. C. Kuo, S. Rostami, J. Matthews, M. Sanada, L. Z. Liu, Y. Shiraishi, S. Miyano, E. Chendamarai, H. A. Hou, G. Malnassy, T. Ma, M. Garg, L. W. Ding, Q. Y. Sun, W. Chien, T. Ikezoe, M. Lill, A. Biondi, R. A. Larson, B. L. Powell, M. Lubbert, W. J. Chng, H. F. Tien, M. Heuser, A. Ganser, M. Koren-Michowitz, S. M. Kornblau, H. M. Kantarjian, D. Nowak, W. K. Hofmann, H. Yang, W. Stock, A. Ghavamzadeh, K. Alimoghaddam, T. Haferlach, S. Ogawa, L. Y. Shih, V. Mathews and H. P. Koeffler (2016). "Comprehensive mutational analysis of primary and relapse acute promyelocytic leukemia." Leukemia **30**(12): 2430.
Martens, J. H., A. B. Brinkman, F. Simmer, K. J. Francoijs, A. Nebbioso, F. Ferrara, L. Altucci and H. G. Stunnenberg (2010). "PML-RARalpha/RXR Alters the Epigenetic Landscape in Acute Promyelocytic Leukemia." Cancer Cell **17**(2): 173-185.
Matic, I., M. van Hagen, J. Schimmel, B. Macek, S. C. Ogg, M. H. Tatham, R. T. Hay, A. I. Lamond, M. Mann and A. C. Vertegaal (2008). "In vivo identification of human small ubiquitin-like modifier polymerization sites by high accuracy mass spectrometry and an in vitro to in vivo strategy." Mol Cell Proteomics **7**(1): 132-144.
Meyer, H. J. and M. Rape (2014). "Enhanced protein degradation by branched ubiquitin chains." Cell **157**(4): 910-921.
Mi, J. Q., S. J. Chen, G. B. Zhou, X. J. Yan and Z. Chen (2015). "Synergistic targeted therapy for acute promyelocytic leukaemia: a model of translational research in human cancer." J Intern Med **278**(6): 627-642.
Mikesch, J. H., H. Gronemeyer and C. W. So (2010). "Discovery of novel transcriptional and epigenetic targets in APL by global ChIP analyses: Emerging opportunity and challenge." Cancer Cell **17**(2): 112-114.
Muller, S., M. J. Matunis and A. Dejean (1998). "Conjugation with the ubiquitin-related modifier SUMO-1 regulates the partitioning of PML within the nucleus." Embo J **17**(1): 61-70.

Perry, J. J., J. A. Tainer and M. N. Boddy (2008). "A SIM-ultaneous role for SUMO and ubiquitin." Trends Biochem Sci **33**(5): 201-208.
Rojas-Fernandez, A., A. Plechanovova, N. Hattersley, E. Jaffray, M. H. Tatham and R. T. Hay (2014). "SUMO chain-induced dimerization activates RNF4." Mol Cell **53**(6): 880-892.
Schindelin, J., I. Arganda-Carreras, E. Frise, V. Kaynig, M. Longair, T. Pietzsch, S. Preibisch, C. Rueden, S. Saalfeld, B. Schmid, J. Y. Tinevez, D. J. White, V. Hartenstein, K. Eliceiri, P. Tomancak and A. Cardona (2012). "Fiji: an open-source platform for biological-image analysis." Nat Methods **9**(7): 676-682.
Schneider, C. A., W. S. Rasband and K. W. Eliceiri (2012). "NIH Image to ImageJ: 25 years of image analysis." Nat Methods **9**(7): 671-675.
Shevchenko, A., H. Tomas, J. Havlis, J. V. Olsen and M. Mann (2006). "In-gel digestion for mass spectrometric characterization of proteins and proteomes." Nat Protoc **1**(6): 2856-2860.
Swedlow, J. R., J. W. Sedat and D. A. Agard (1996). Deconvolution in optical microscopy Deconvolution of Images and Spectra (2nd Ed). USA, Academic Press, Inc.**:** 284-309.
Tammsalu, T., I. Matic, E. G. Jaffray, A. F. Ibrahim, M. H. Tatham and R. T. Hay (2014). "Proteome-wide identification of SUMO2 modification sites." Sci Signal **7**(323): rs2.
Tan, Y., X. Wang, H. Song, Y. Zhang, R. Zhang, S. Li, W. Jin, S. Chen, H. Fang, Z. Chen and K. Wang (2021). "A PML/RARalpha direct target atlas redefines transcriptional deregulation in acute promyelocytic leukemia." Blood **137**(11): 1503-1516.
Tatham, M. H., M. C. Geoffroy, L. Shen, A. Plechanovova, N. Hattersley, E. G. Jaffray, J. J. Palvimo and R. T. Hay (2008). "RNF4 is a poly-SUMO-specific E3 ubiquitin ligase required for arsenic-induced PML degradation." Nat Cell Biol **10**(5): 538-546.
Tatham, M. H., E. Jaffray, O. A. Vaughan, J. M. Desterro, C. H. Botting, J. H. Naismith and R. T. Hay (2001). "Polymeric chains of SUMO-2 and SUMO-3 are conjugated to protein substrates by SAE1/SAE2 and Ubc9." J Biol Chem **276**(38): 35368-35374.
Twomey, E. C., Z. Ji, T. E. Wales, N. O. Bodnar, S. B. Ficarro, J. A. Marto, J. R. Engen and T. A. Rapoport (2019). "Substrate processing by the Cdc48 ATPase complex is initiated by ubiquitin unfolding." Science **365**(6452).
Tyanova, S., T. Temu, P. Sinitcyn, A. Carlson, M. Y. Hein, T. Geiger, M. Mann and J. Cox (2016). "The Perseus computational platform for comprehensive analysis of (prote)omics data." Nat Methods **13**(9): 731-740.
Wallace, W., L. H. Schaefer and J. R. Swedlow (2001). "A workingperson's guide to deconvolution in light microscopy." Biotechniques **31**(5): 1076-1078, 1080, 1082 passim.
Wang, Z. Y. and Z. Chen (2008). "Acute promyelocytic leukemia: from highly fatal to highly curable." Blood **111**(5): 2505-2515.
Weis, K., S. Rambaud, C. Lavau, J. Jansen, T. Carvalho, M. Carmo-Fonseca, A. Lamond and A. Dejean (1994). "Retinoic acid regulates aberrant nuclear localization of PML-RAR alpha in acute promyelocytic leukemia cells." Cell **76**(2): 345-356.
Yau, R. G., K. Doerner, E. R. Castellanos, D. L. Haakonsen, A. Werner, N. Wang, X. W. Yang, N. Martinez-Martin, M. L. Matsumoto, V. M. Dixit and M. Rape (2017). "Assembly and Function of Heterotypic Ubiquitin Chains in Cell-Cycle and Protein Quality Control." Cell **171**(4): 918-933 e920.
Zhu, H. H., Y. Z. Qin and X. J. Huang (2014). "Resistance to arsenic therapy in acute promyelocytic leukemia." N Engl J Med **370**(19): 1864-1866.

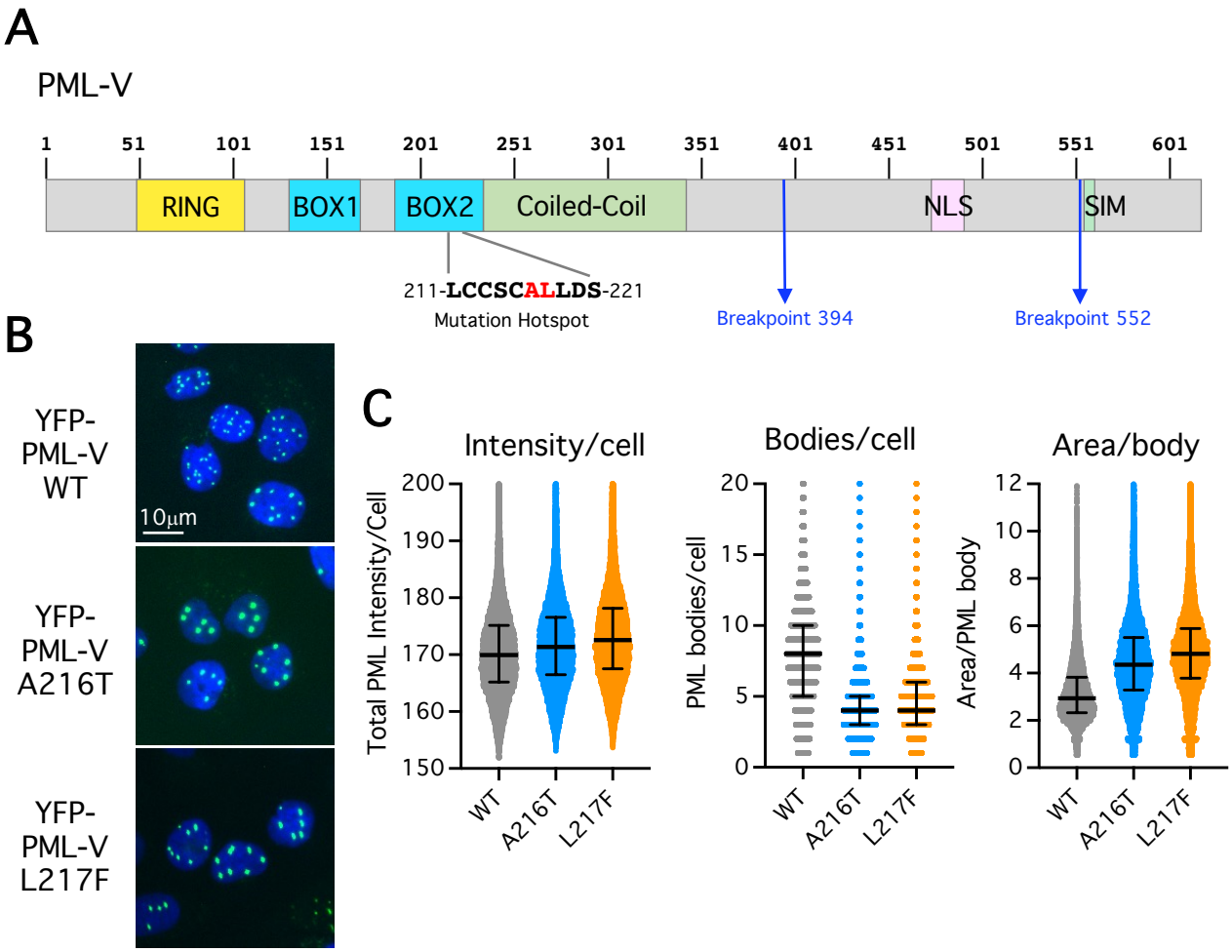

Figure 1. Jaffray et al 2023

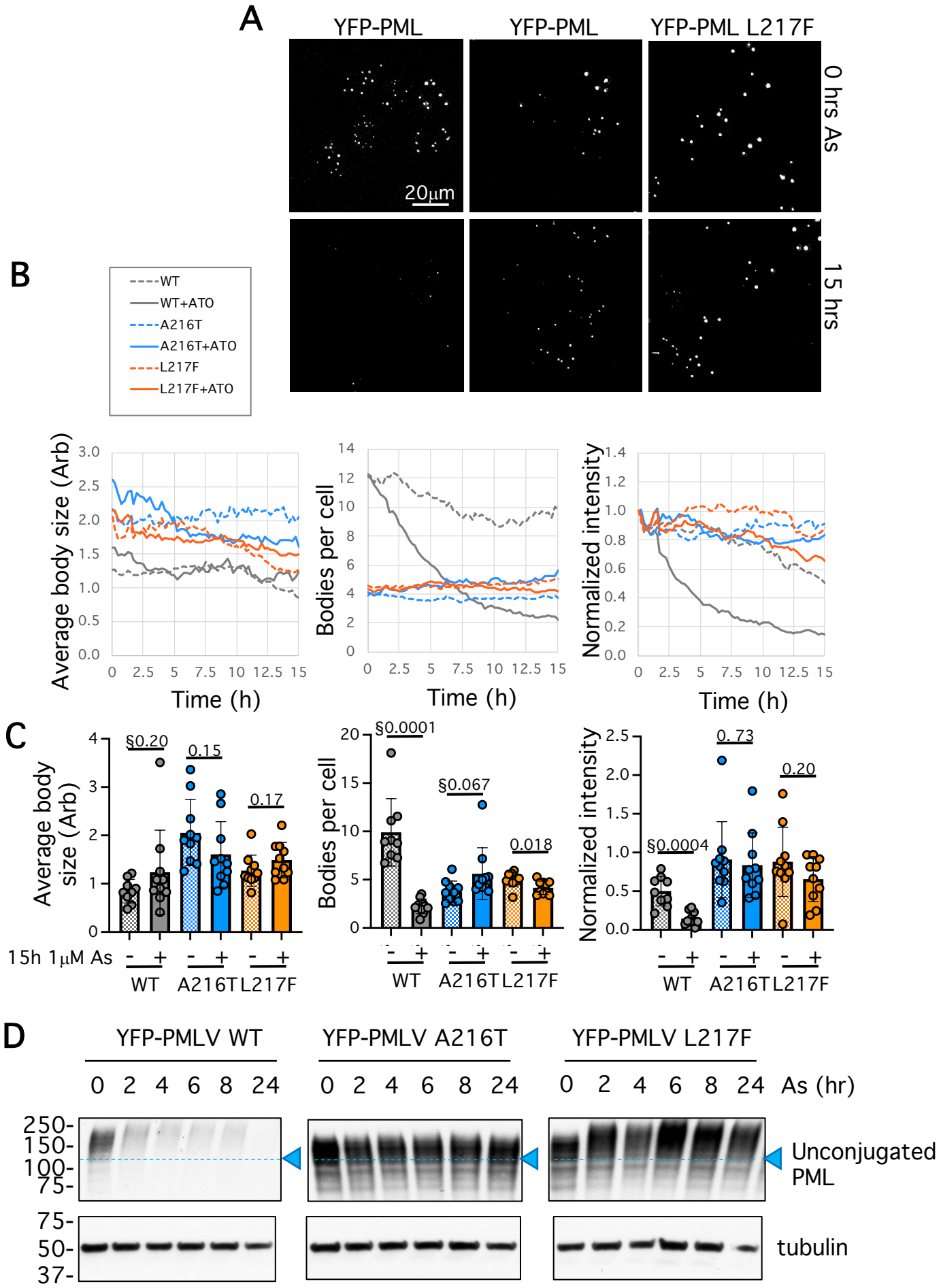

Figure 2. Jaffray et al 2023

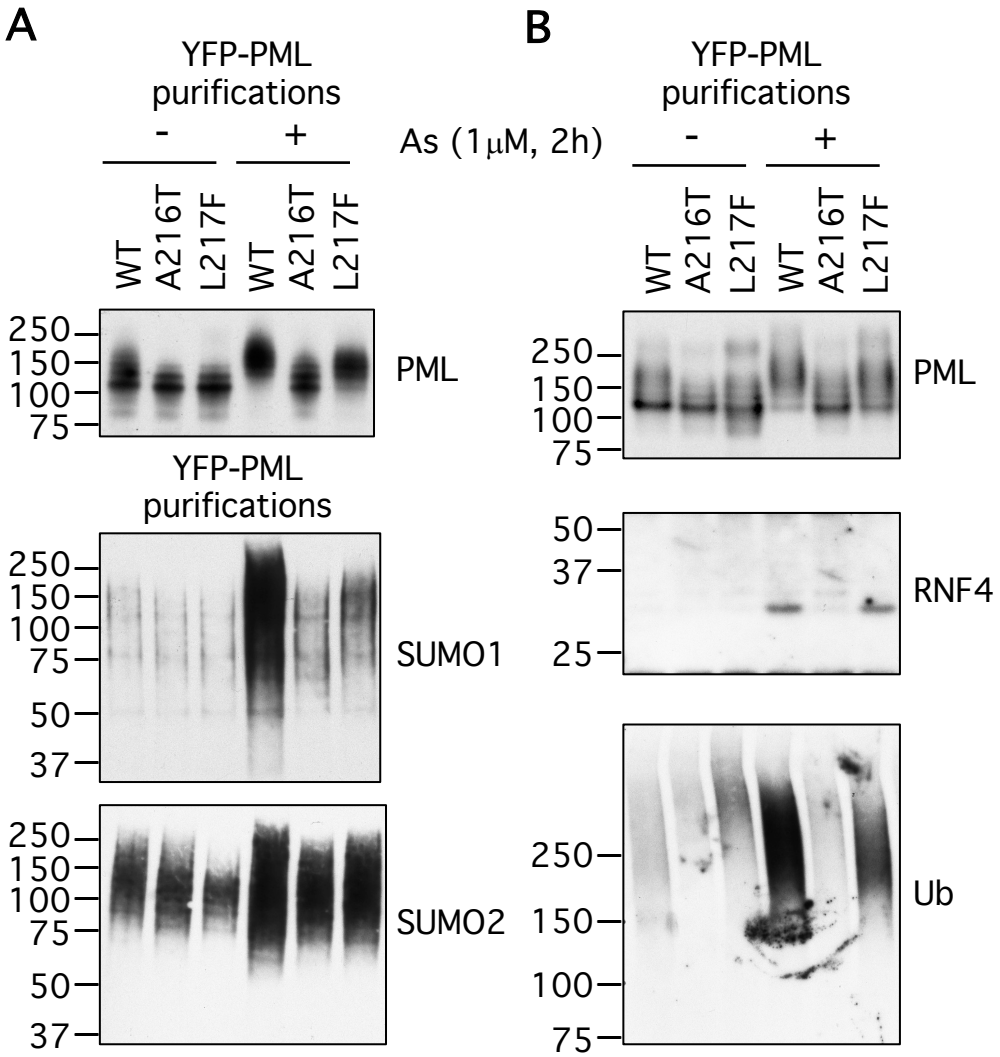

Figure 3. Jaffray et al 2023

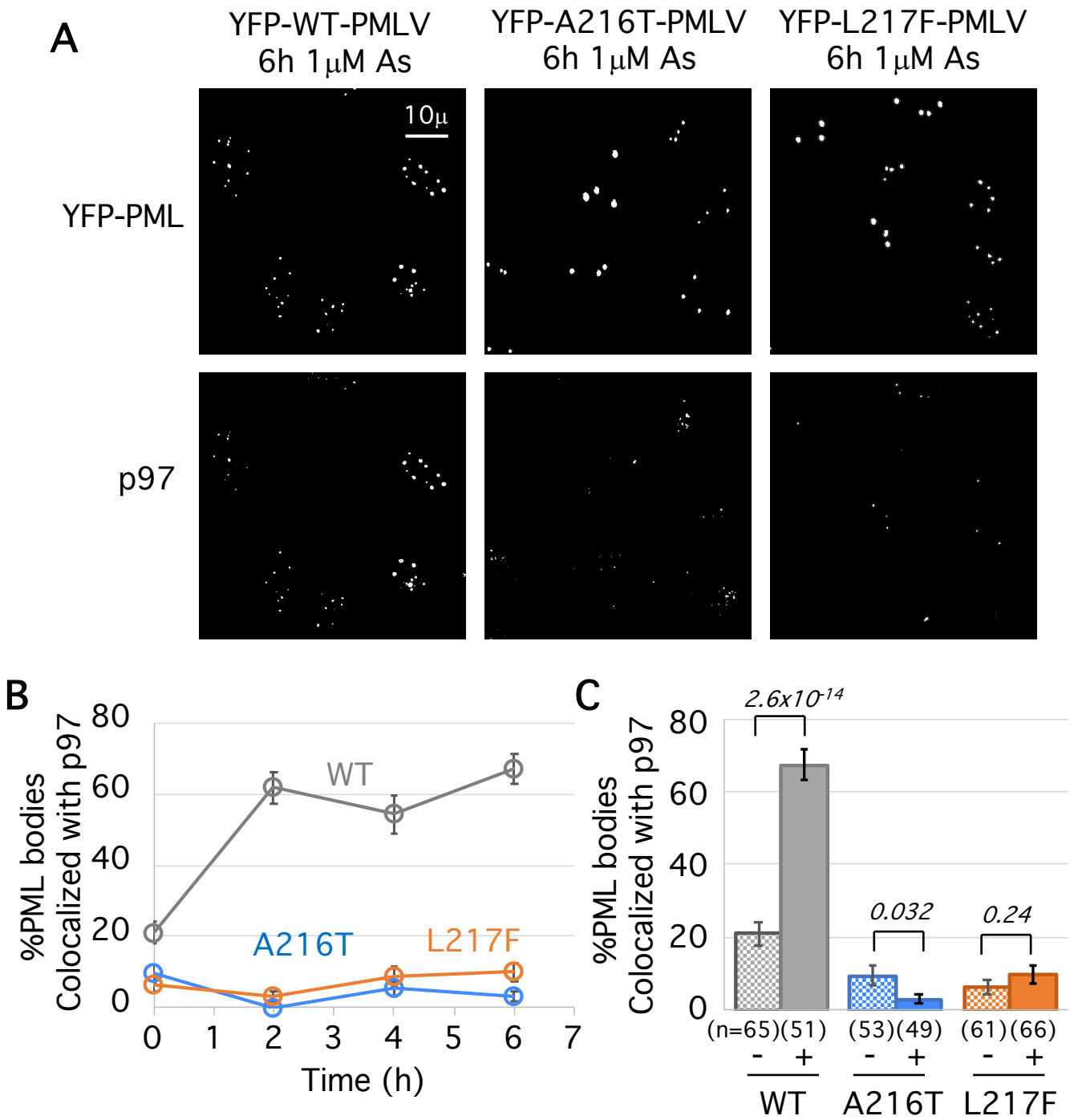

Figure 4. Jaffray et al 2023

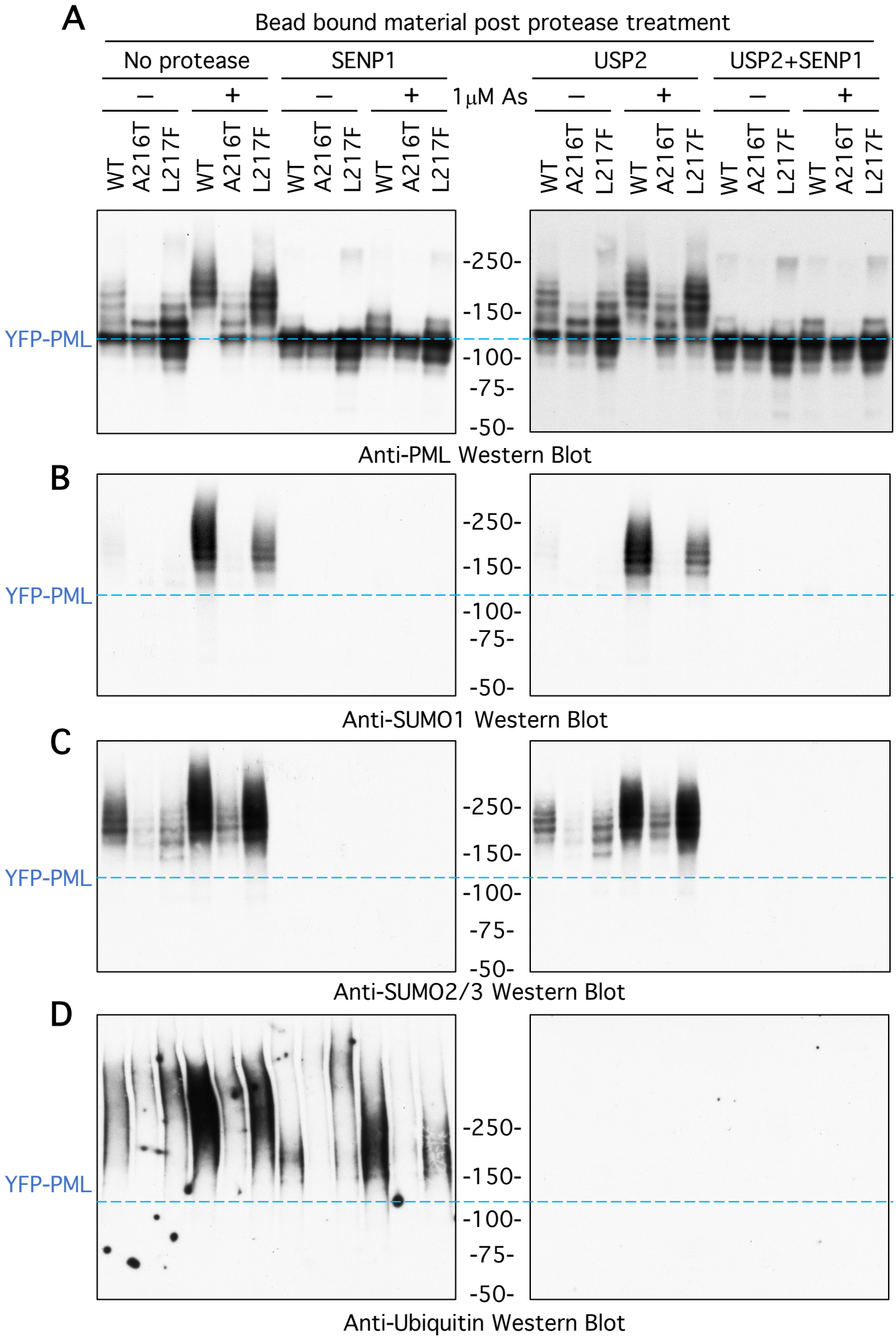

Figure 5. Jaffray et al 2023

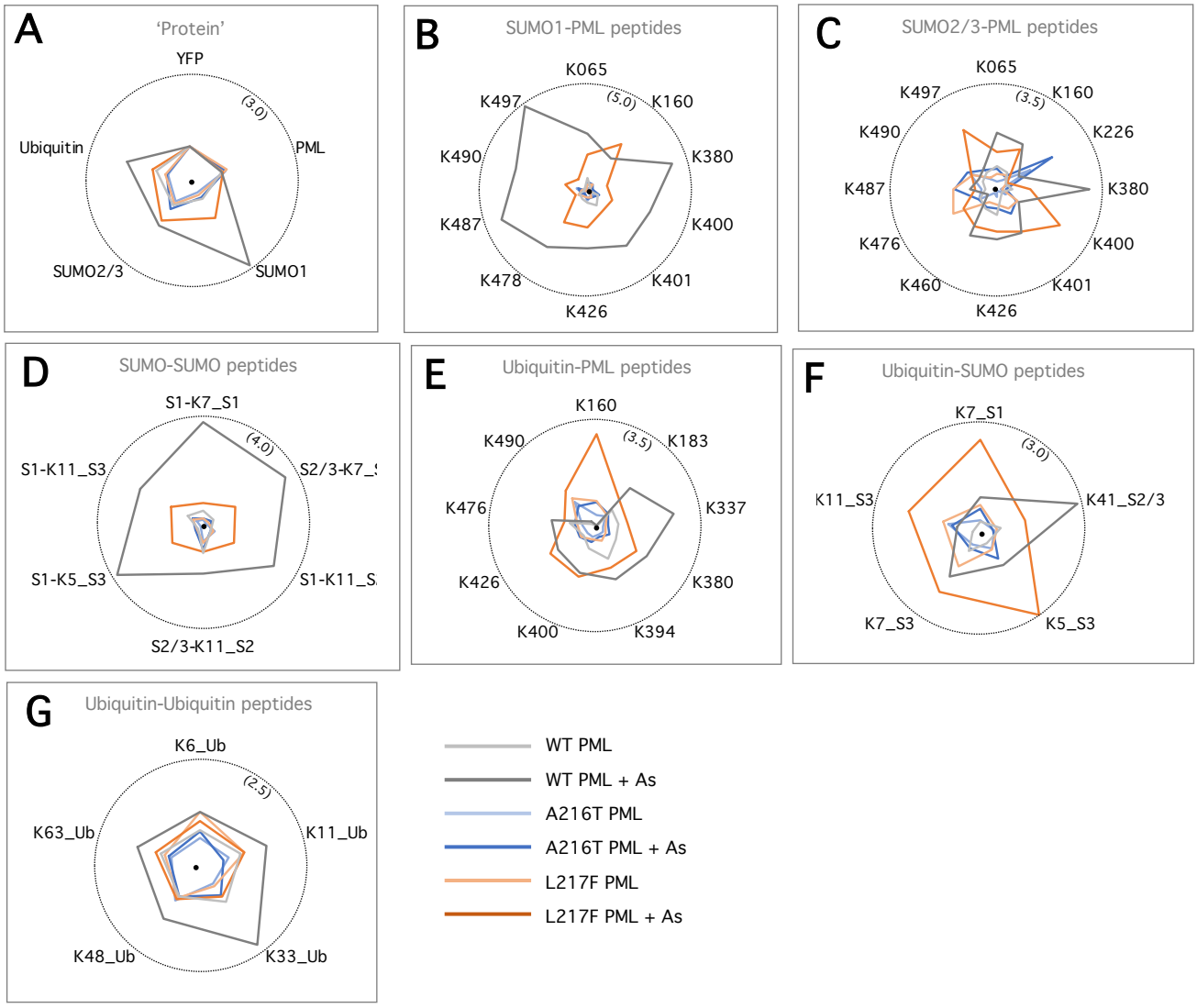

Figure 6. Jaffray et al 2023

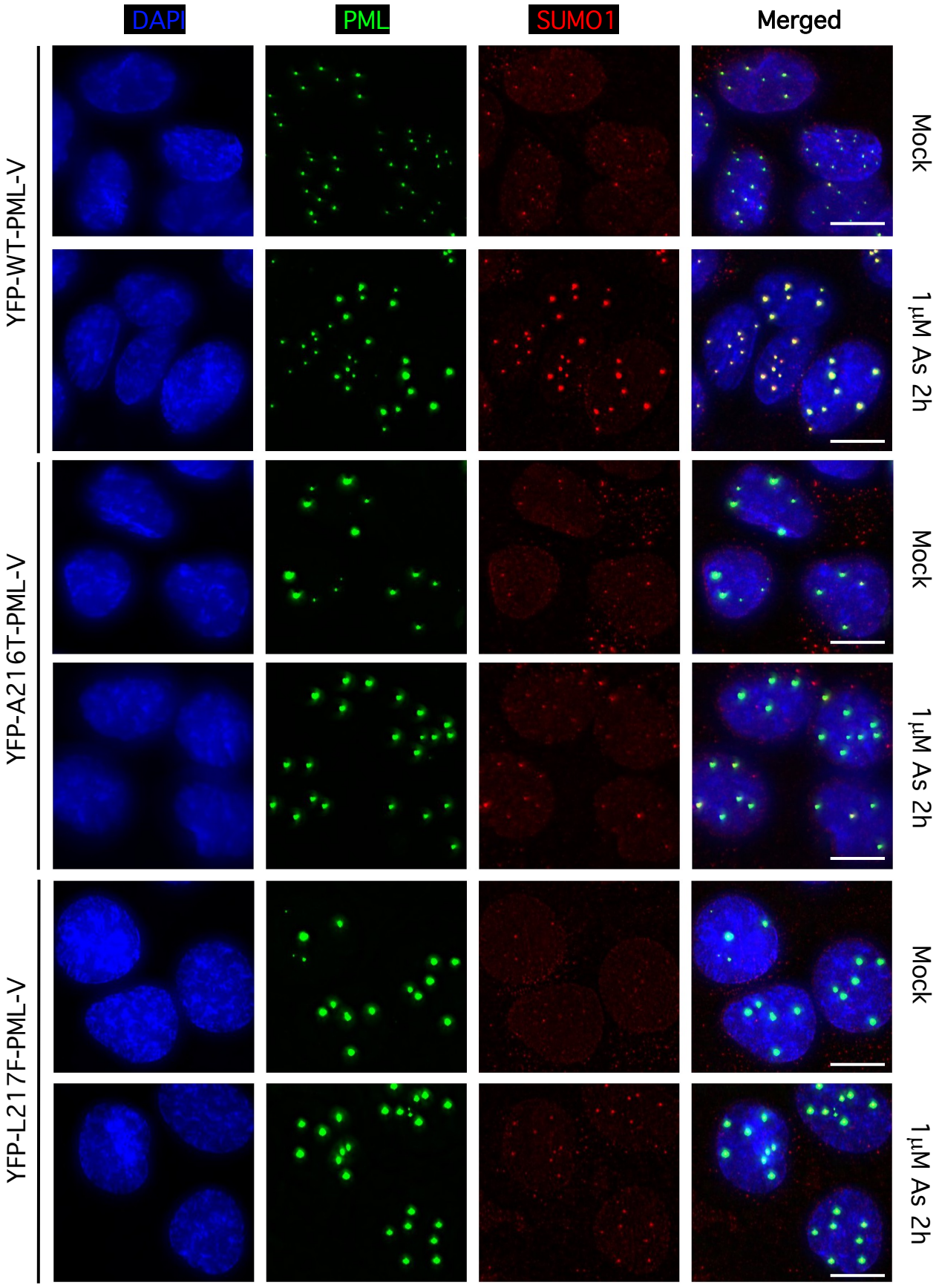

Supplementary Figure 1. Jaffray et al 2023

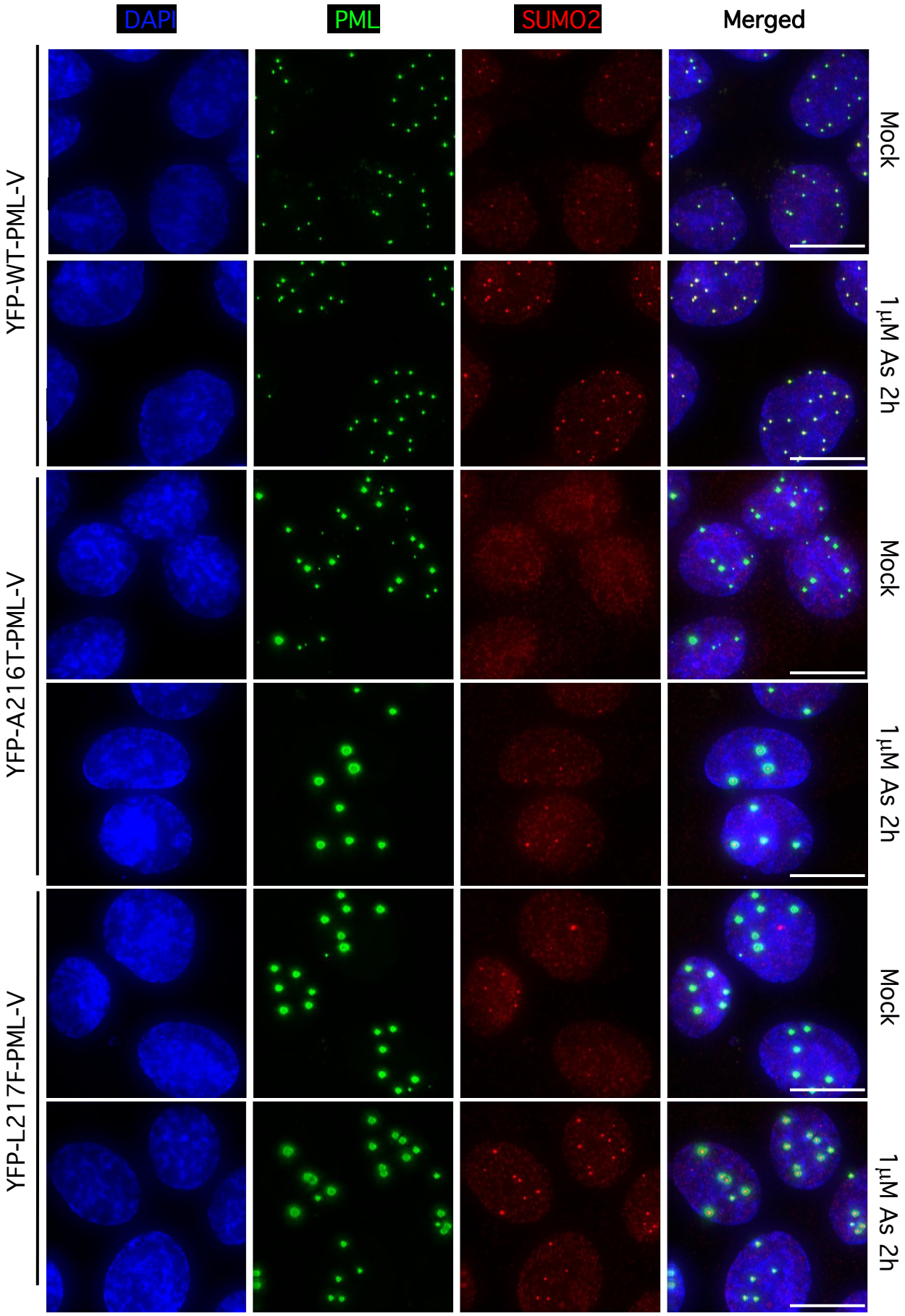

Supplementary Figure 2. Jaffray et al 2023

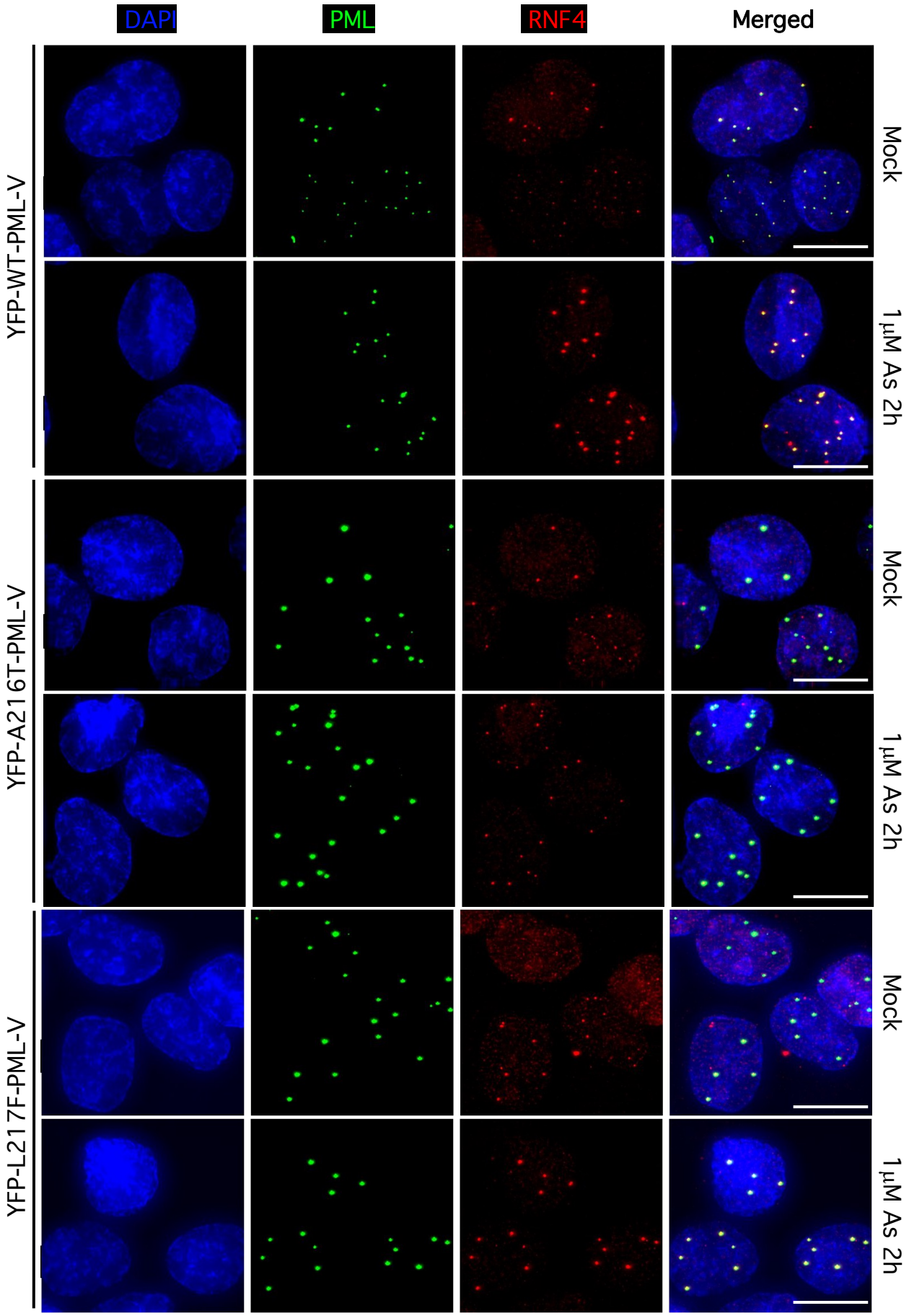

Supplementary Figure 3. Jaffray et al 2023

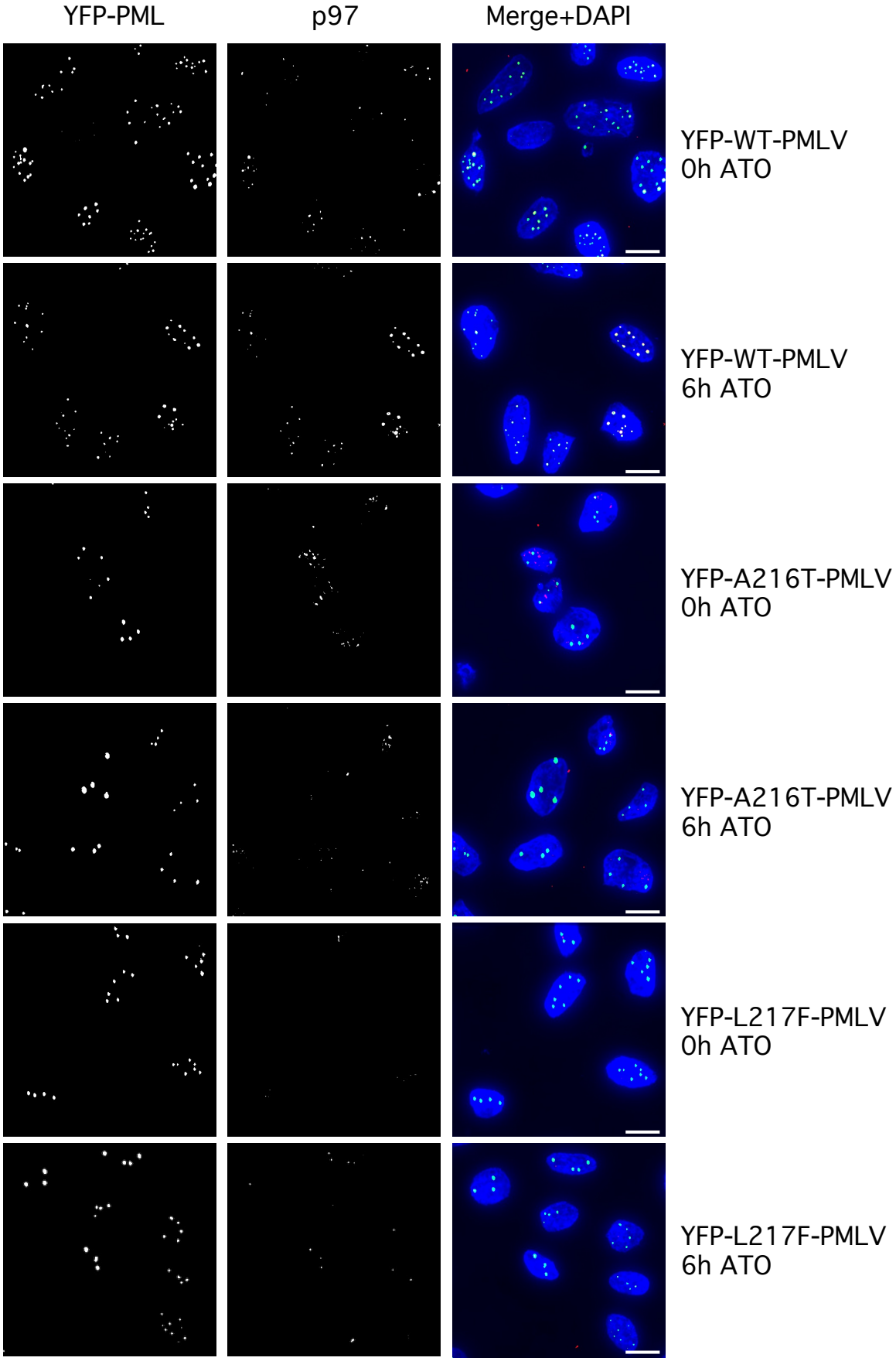

Supplementary Figure 4. Jaffray et al 2023

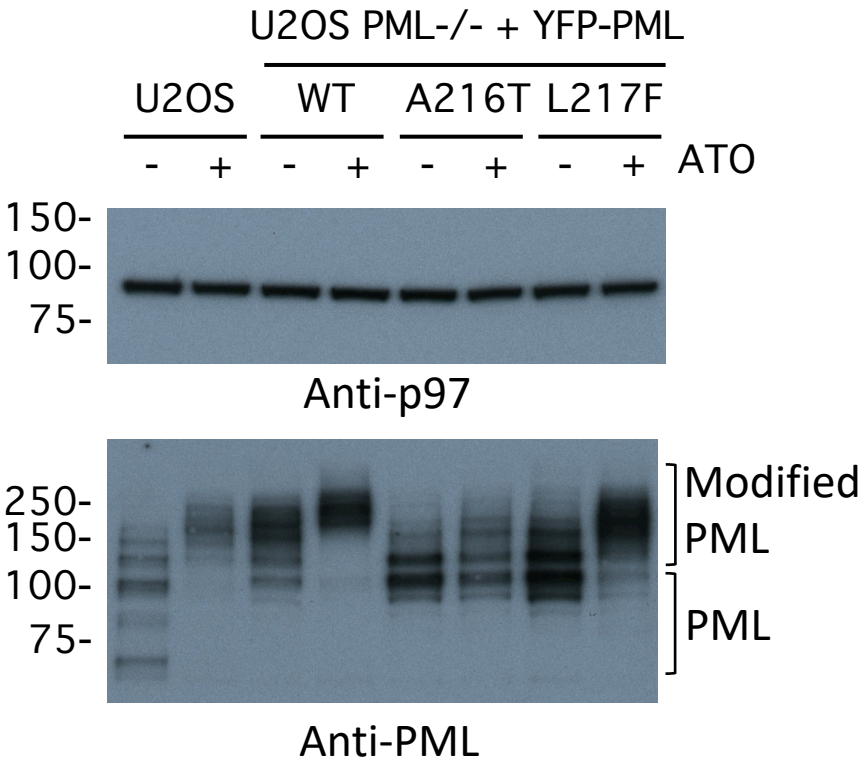

Supplementary Figure 5. Jaffray et al 2023

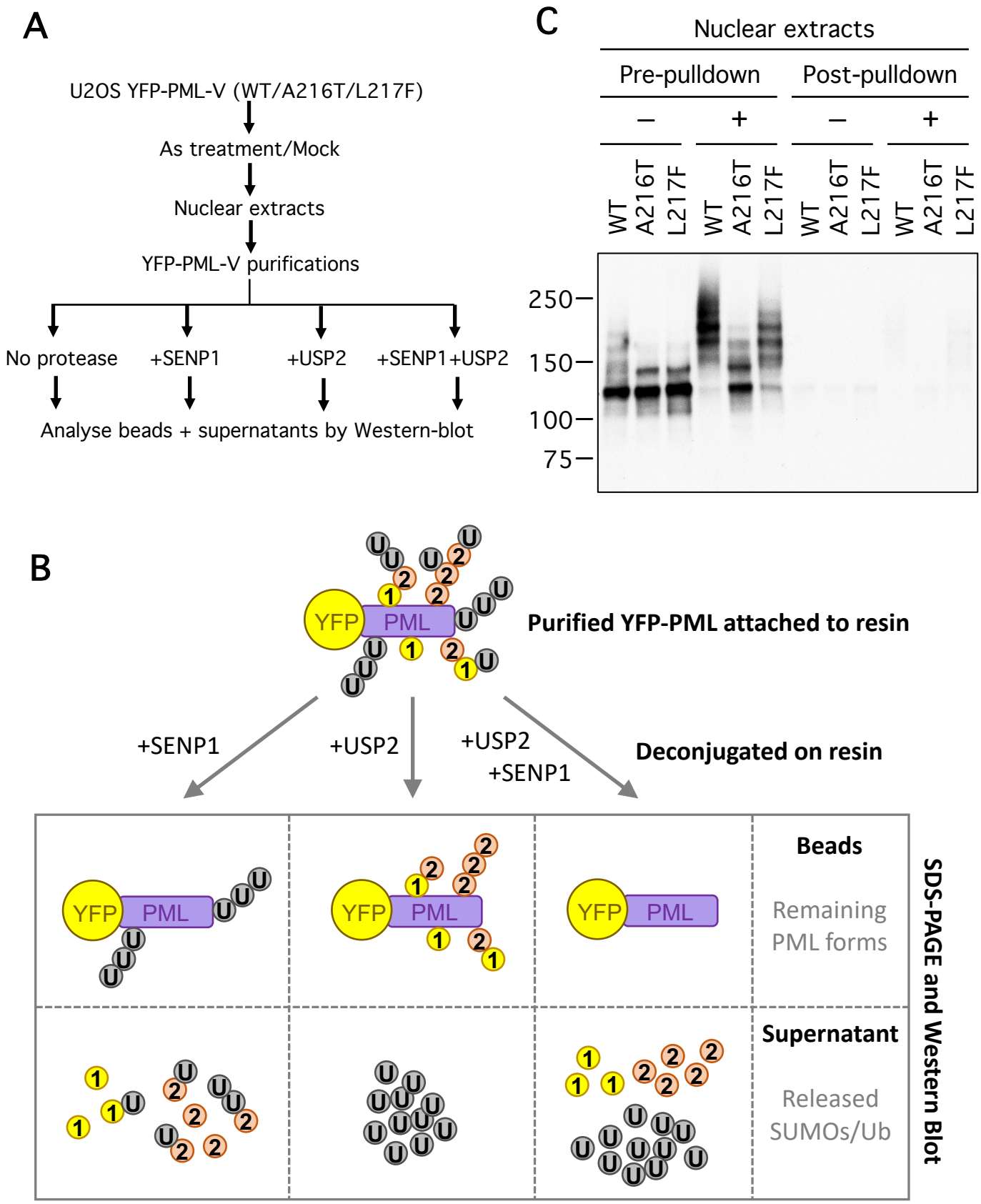

Supplementary Figure 6. Jaffray et al 2023

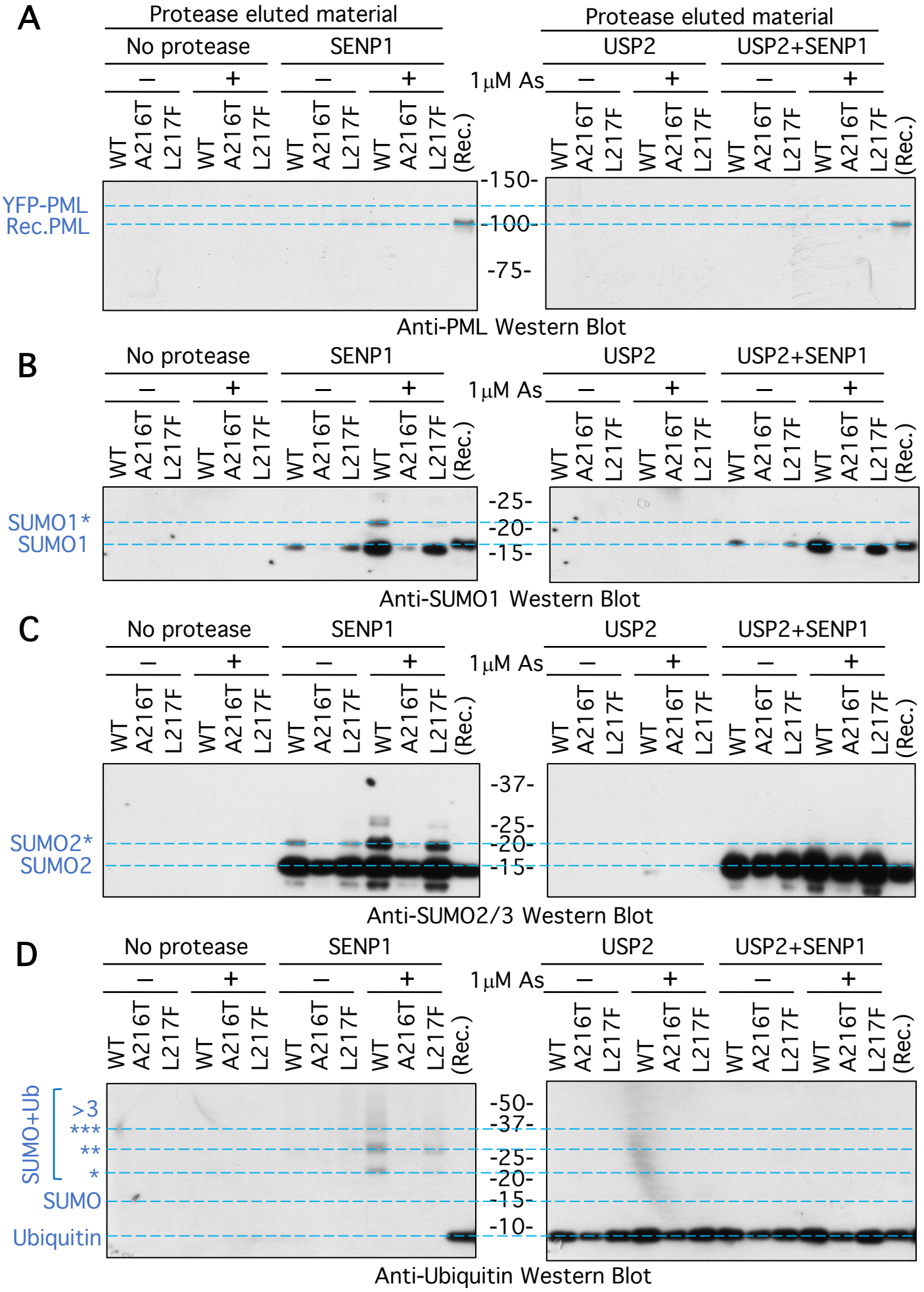

Supplementary Figure 7. Jaffray et al 2023

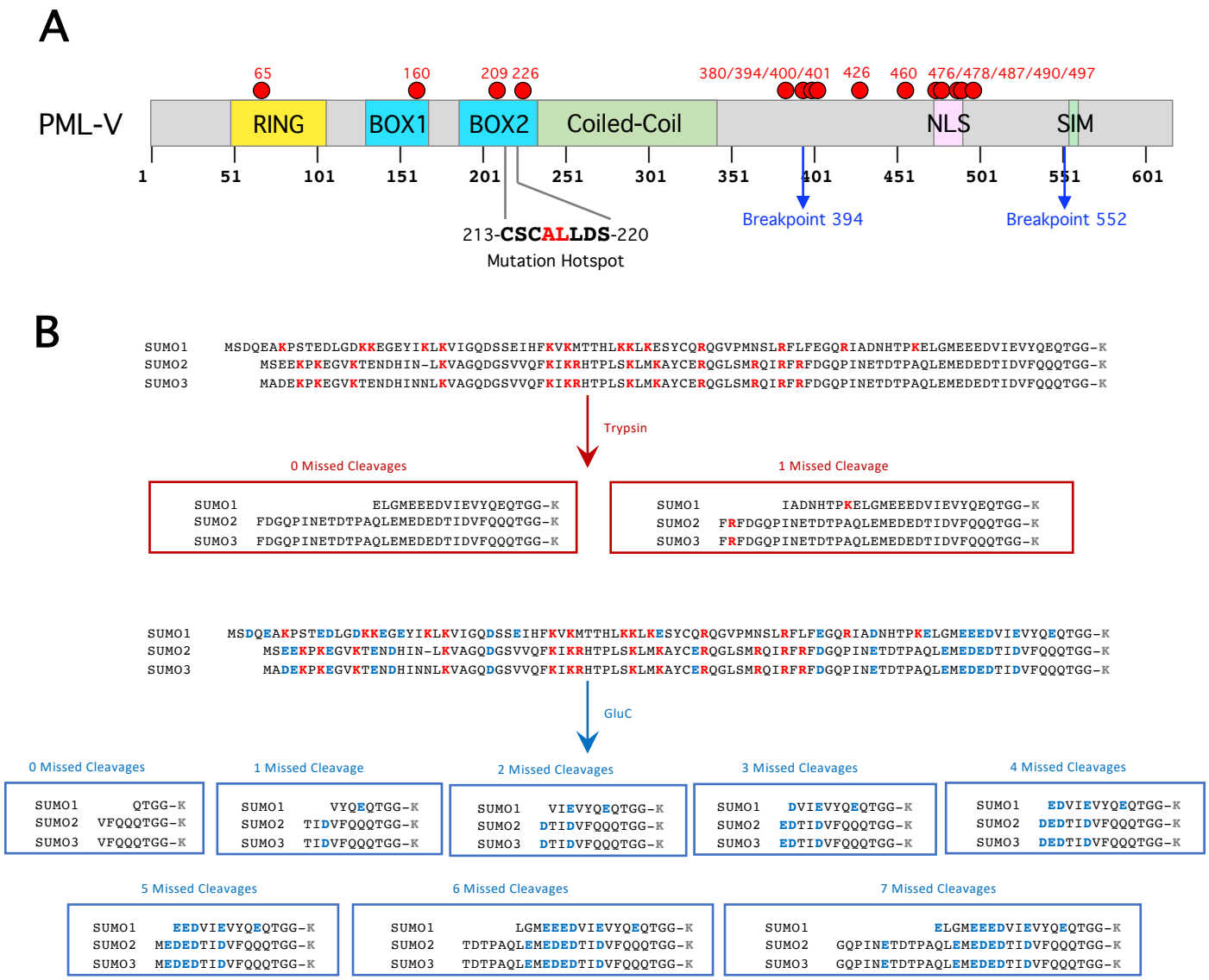

Supplementary Figure 8. Jaffray et al 2023

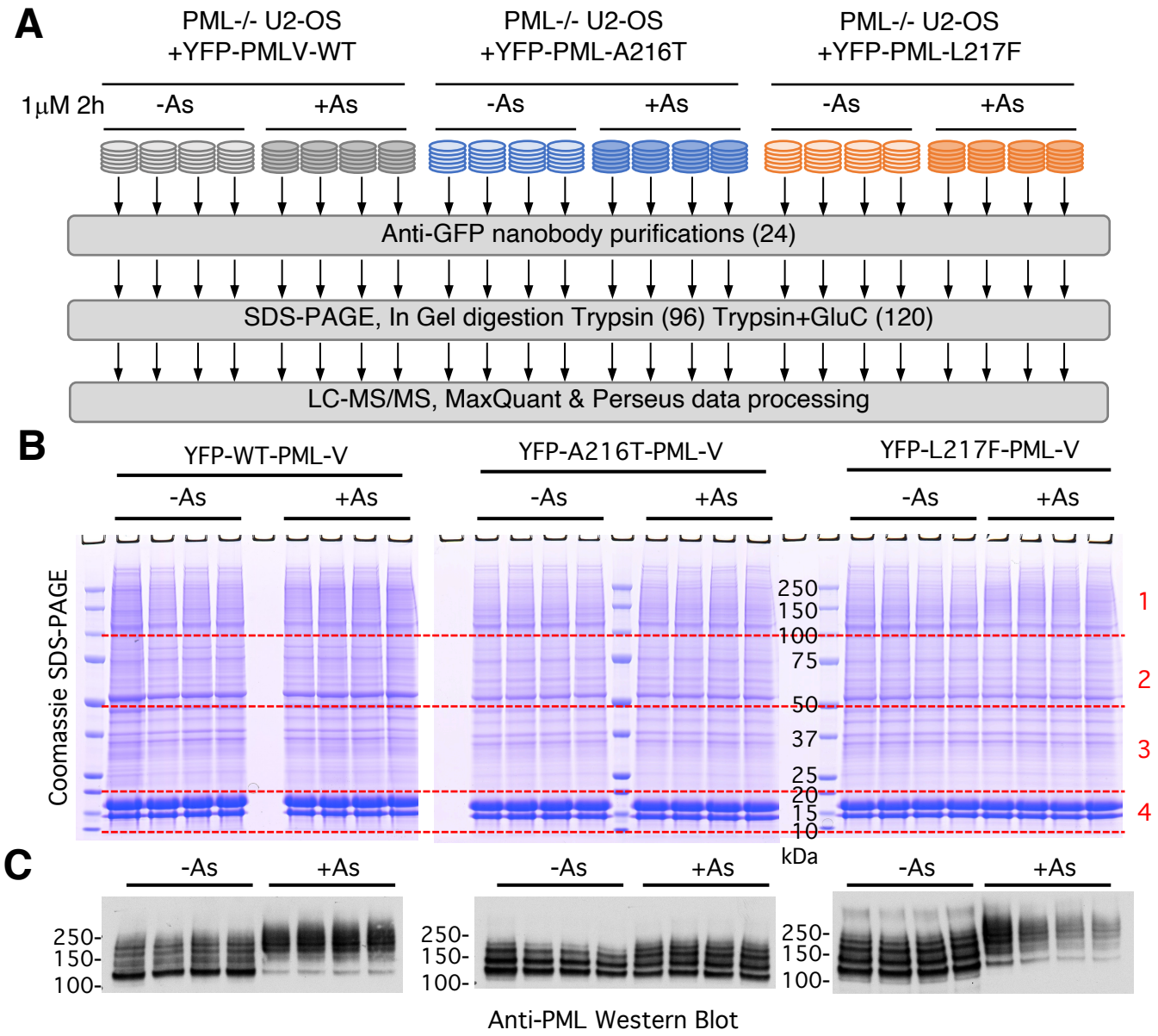

Supplementary Figure 9. Jaffray et al 2023

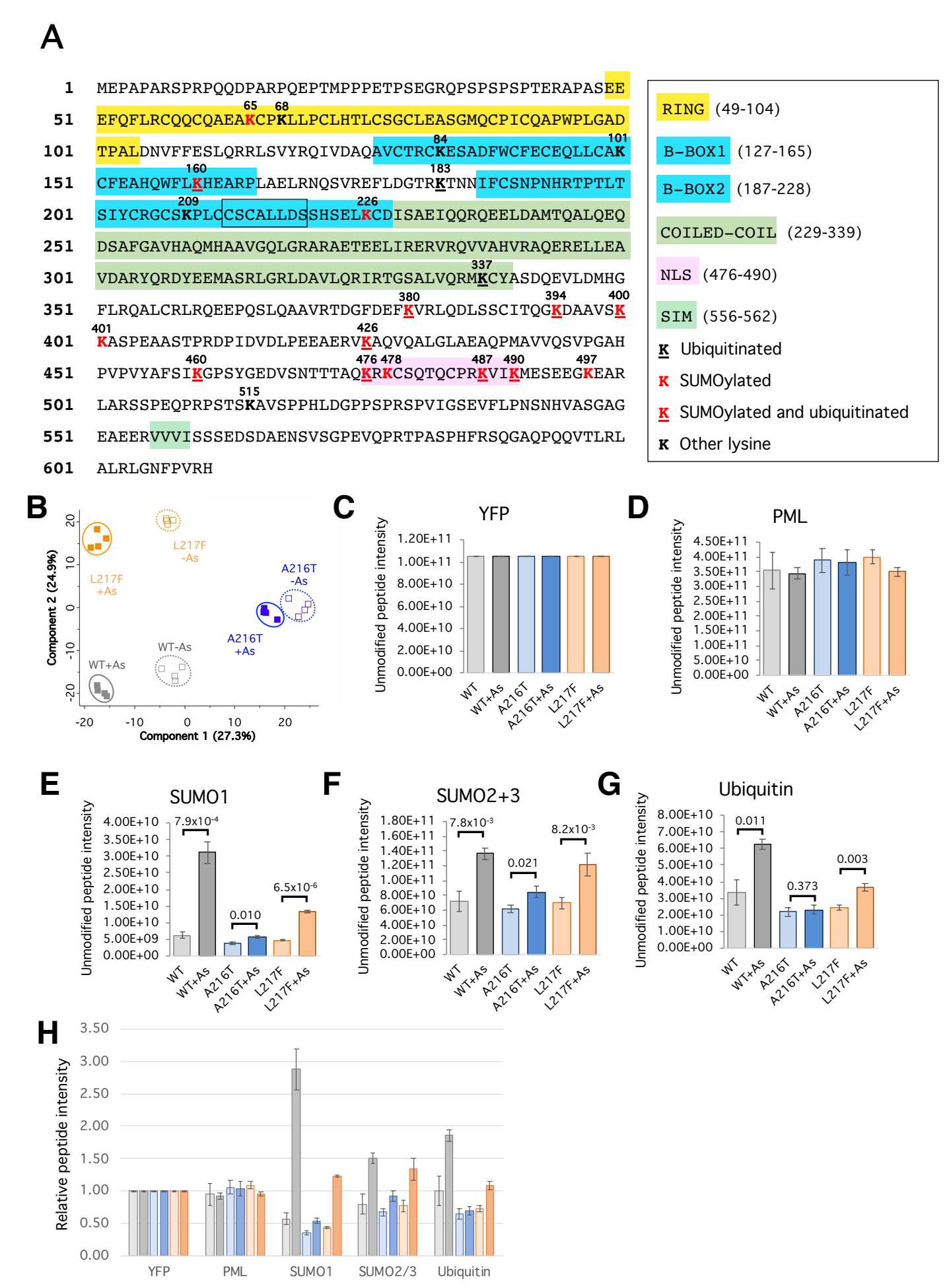

Supplementary Figure 10. Jaffray et al 2023

A. Unmodified counterpart peptides

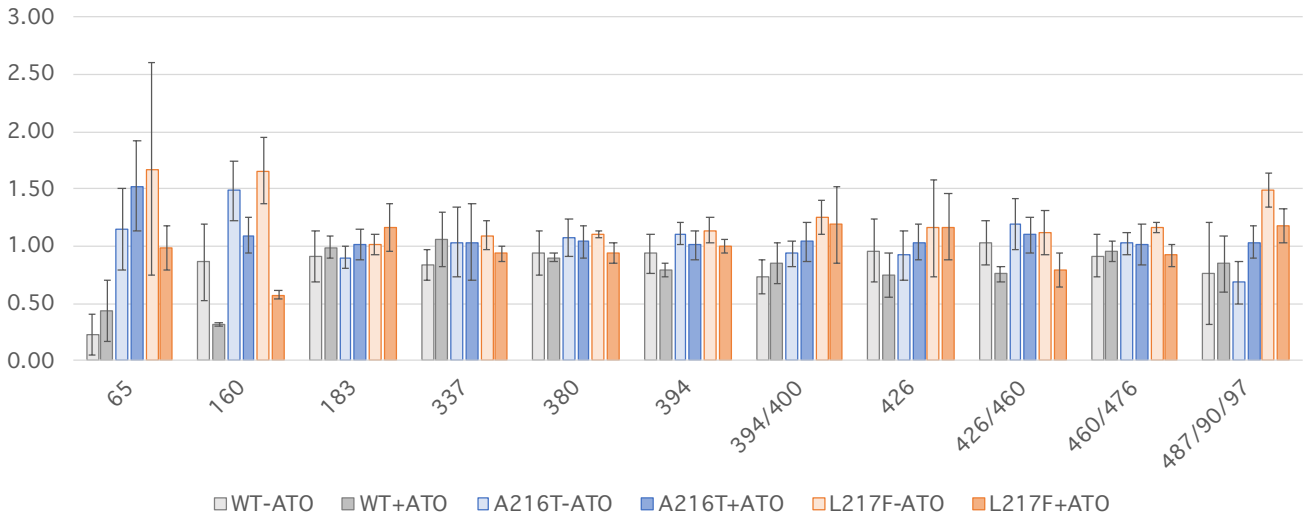

B. Ubiquitin-Ubiquitin branched peptides

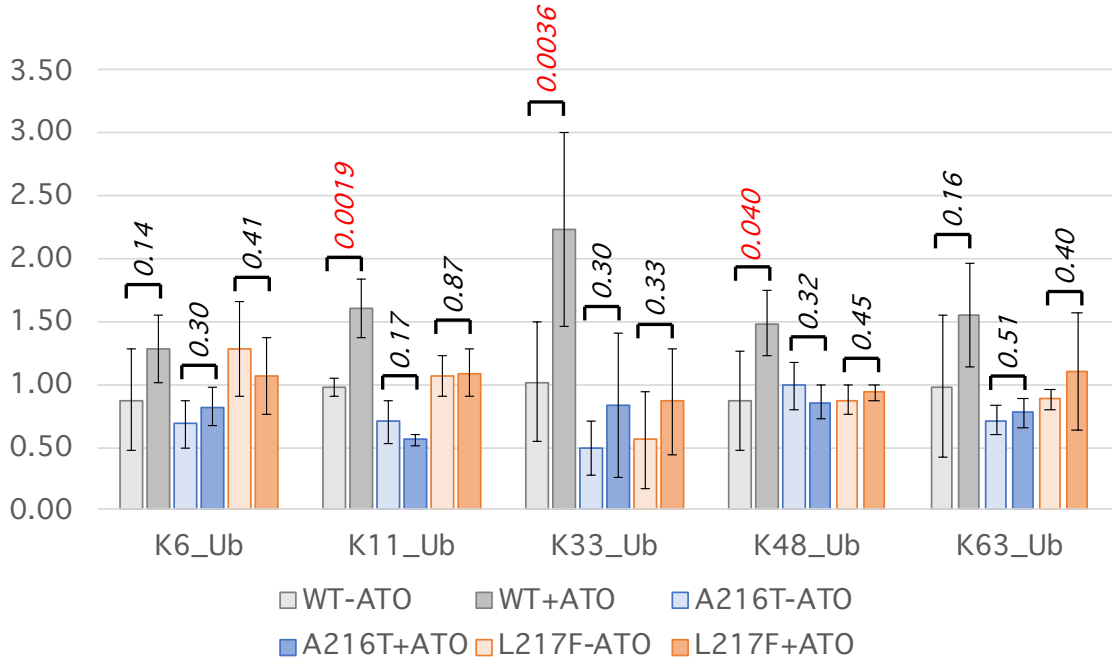

Supplementary Figure 11. Jaffray et al 2023

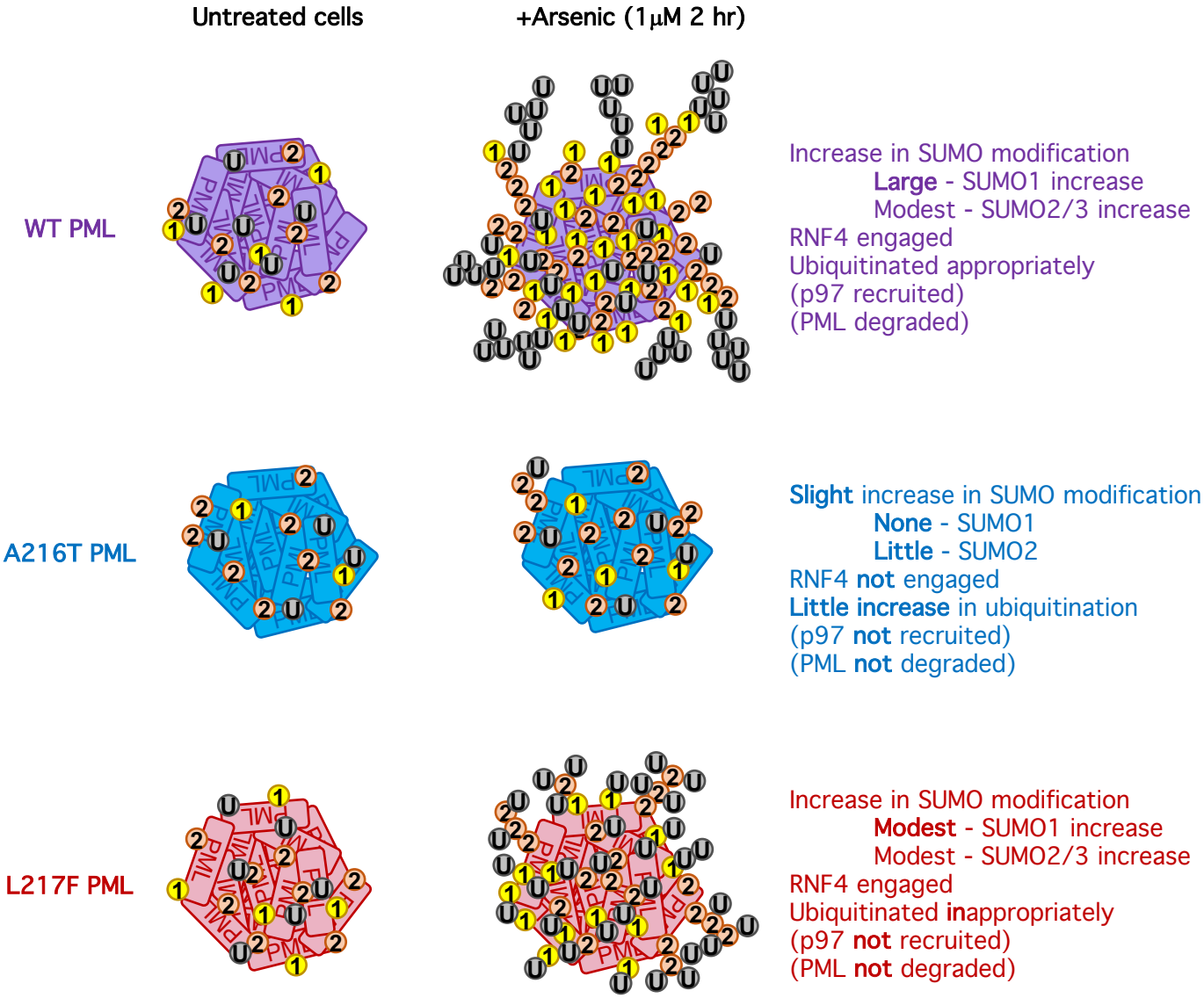

Supplementary Figure 11. Jaffray et al 2023